# PHOSPHORUS REMOVAL FROM MANGANESE ORE

# BY PLASMA TREATMENT

by

Su Hyun Hwang

A thesis submitted to the faculty of
The University of Utah
in partial fulfillment of the requirements for the degree of

Master of Science

Department of Metallurgical Engineering

The University of Utah

August 2011

**The University of Utah Graduate School**

# STATEMENT OF THESIS APPROVAL

The thesis of **Su Hyun Hwang**

has been approved by the following supervisory committee members:

| | | |
|---|---|---|
| **Hong Yong Sohn** | , Chair | **April 18, 2011** Date Approved |
| **Hang Goo Kim** | , Member | **April 18, 2011** Date Approved |
| **Zhigang Zak Fang** | , Member | **April 18, 2011** Date Approved |

and by **Jan D. Miller** , Chair of

the Department of **Metallurgical Engineering**

and by Charles A. Wight, Dean of The Graduate School.

## ABSTRACT

The contents of impurities, especially that of phosphorus, in manganese metal or in ferromanganese used in steelmaking are an important factor that affects product quality. More than 80% of phosphorus in the manganese products is introduced from manganese ore, the rest coming from coke and lime. Once it is absorbed into a molten manganese ore ferromanganese phase, it cannot be easily removed by smelting, and thus, ferromanganese must generally be low in phosphorus to begin with. As good quality ores of low phosphorus are depleted, the phosphorus content in manganese ores increases, and thus, the development of a new dephosphorization technology is needed.

For this purpose, the removal of phosphorus compounds by vaporization directly from manganese ores using a plasma system was investigated in this study. For the removal of phosphorus, the effects of argon gas flow rate, hydrogen gas content in the plasma gas, and plasma torch power were analyzed. In addition, based on the thermal decomposition of hematite in the ores into magnetite at a high temperature, a magnetic separation was conducted after plasma treatment aiming to upgrade manganese ores. For the removal of phosphorus, a low argon gas flow rate and a high torch power were found to be effective, and the use of hydrogen gas as a reducing agent was more favorable than without. Magnetic separation after plasma treatment improved the ore grade with a decrease of iron content in the ore.

**TABLE OF CONTENTS**

## LIST OF FIGURES

## LIST OF TABLES

## ACKNOWLEDGMENTS

I wish to express my gratitude to all those who have helped and encouraged me throughout my study at the University of Utah. My deepest thanks to my supervisor, Professor H. Y. Sohn, whose encouragement and valuable advice enabled me to accomplish this work.

I am grateful to the other committee members, Professor H. G. Kim and Professor Z. Z. Fang, for their advice and guidance. I am also grateful to Professor D. Y. Lim of Pai Chai University for extending his support.

I am thankful to Dr. Chang Hun Keum, Dr. Moo Eob Choi, Mr. Kyu Sup Hwang, Mr. Miguel Olivas-Martinez, and Mr. Tyler Bronson for their help.

It would not have been possible to complete this work without the love and support of my family. Especially, I owe my deepest gratitude to my wife for her love and patience.

This work was supported financially by the Research Institute of Industrial Science and Technology, Pohang, Korea.

# 1. INTRODUCTION

Manganese is an essential element for making steel. After iron, aluminum, and copper, manganese ranks along with zinc as the next most used metal in the world. Manganese is widely distributed in many mineral forms constituting about 0.1% of the earth's crust and is the 12$^{th}$ most abundant element.[1-4]

About 90 to 95% of world manganese production is used in iron and steel industries. In steelmaking, ferromanganese (Fe-Mn) alloy is used as a deoxidizer and desulphuriser. Because it has a higher oxygen and sulfur affinity than Fe, Mn reacts with remaining oxygen and sulfur in the steel forming MnO and MnS, respectively, and then is separated from molten steel into slag, while Fe in the Fe-Mn is dissolved into the molten steel. In addition, manganese improves strength, toughness, hardness, and workability of steel as an alloying element.

The contents of impurities, especially phosphorus, in ferromanganese are an important factor which should be controlled in steelmaking. Phosphorus is a deleterious contaminant because it makes steel brittle, even at a concentration as low as 0.6%. More than 80% of phosphorus in the Fe-Mn alloy comes from the manganese ore, the rest coming from coke and lime. Because phosphorus is nobler than Mn and has a high affinity to Fe, almost all P is absorbed into Fe-Mn alloy during the direct reduction of the ore by carbon in the smelting process. Therefore, phosphorus cannot be easily removed

by smelting, and thus, manganese metal or ferromanganese must generally be low in phosphorus to begin with.

While the demand for high quality steel of low phosphorus increases, the phosphorus content in manganese ores increases as good quality ores of low phosphorus are depleted. To this date, the control of phosphorus has been mainly achieved by a slag-metal partitioning process with a basic slag using BaO or $BaCO_3$ under oxidizing atmosphere or using $CaC_2$ or metallic Ca under reducing atmosphere.[5-9] For these processes, however, too much loss of manganese (large slag loss at oxidizing atmosphere while large dust loss at reducing atmosphere) is caused and the prices of the fluxes are quite expensive. Therefore, the development of a new dephosphorization technology which can overcome the above problems is needed.

For this purpose, as an alternative technology, the removal of phosphorus compounds by vaporization directly from manganese ores at high temperatures is investigated based on the fact that phosphorus can form several volatile compounds such as PO and $PO_2$ in an oxidizing atmosphere and such as $P_2$, $P_4$, and PH in a reducing atmosphere.

In the present study, the use of a thermal plasma system for this object is examined. Plasma processing technique has been developed for the coating techniques, synthesis of fine powders, waste destruction, and melting applications. For the removal of impurities, the thermal plasma process provides many advantages such as a high processing temperature, clean reaction atmosphere, and high quench rate. The plasma process covers many industrial applications.[10-17]

The main objective of this research is to study the feasibility of plasma treatment for the removal of phosphorus directly from manganese ores by vaporizing phosphorus compounds. For removal of phosphorus, the effects of experimental conditions such as the plasma gas flow rate (Ar), $H_2$ content in the plasma gas, and plasma torch power are analyzed. In addition, based on the thermal decomposition of hematite in the ores into magnetite at a high temperature, a magnetic separation is conducted after plasma treatment aiming to upgrade manganese ores by reducing iron content in the ore. The effect of magnetic force on the upgrading is also investigated in this study.

# 2. LITERATURE SURVEY AND THEORETICAL STUDY

## 2.1. Ferro-manganese

Manganese is used in iron and steelmaking processes for deoxidation and desulfurization, and alloying. Approximately 95% of manganese ore is consumed in the manufacture of steel as ferromanganese and silicomanganese. The other 5% is used in such other industries as chemical, paint, fertilizer, and battery industries.[18] Manganese is the 12th abundant element in the earth's crust but minable manganese ore is limited to several countries. Table 1 shows the manganese ore production and reserves.[19]

Manganese ores usually contain iron oxides, and in these ores the manganese can occur as $MnO_2$, $Mn_2O_3$, $Mn_3O_4$, and also as $MnSiO_3$. Occasionally $MnO_2$ can occur in a relatively pure form, known as pyrolusite. The various manganese minerals found in these ores are: manganite ($Mn_2O_3$), hausmannite ($Mn_3O_4$), braunite ($3Mn_2O_3 \cdot MnSiO_3$), rhodonite ($MnSiO_3$), and psilomelane ($BaMnMn_8O_{16}(OH)_4$). There are ores containing 45% Mn, but with a Mn:Fe ratio of 4 : 1 to 2 : 1, which are only suitable for blending with higher ratio ores. For making standard ferromanganese (high carbon), the Mn:Fe ratio should be a minimum of 6 to 1.

Crushing, screening, washing, jigging, and tabling, as well as flotation, heavy-media, and high-intensity magnetic separation processes are performed to produce manganese concentrates from low grade manganese ores.[20]

Table 1. Manganese ore production and reserves[19] (gross weight, thousand metric tons)

| Country | 2009 | 2010 | Reserves |
|---|---|---|---|
| Australia | 2,140 | 2,400 | 93,000 |
| Brazil | 730 | 830 | 110,000 |
| China | 2,400 | 2,800 | 44,000 |
| Gabon | 881 | 1,400 | 52,000 |
| India | 980 | 1,100 | 56,000 |
| Mexico | 169 | 210 | 4,000 |
| South Africa | 1,900 | 2,200 | 120,000 |
| Ukraine | 375 | 580 | 140,000 |
| Other | 1,240 | 1,400 | Small |
| Total | 10,800 | 13,000 | 630,000 |

In steelmaking, manganese is usually added in the form of a ferroalloy. This includes three grades of ferromanganese (Fe-Mn) – standard (high-carbon – HC) grade containing 74-82% Mn and 7.5% carbon; refined grades with medium-carbon (MC) and low-carbon (LC); and silicomanganese (Si-Mn), which contains 65-68% Mn and around 2% carbon. Cost, the type of steel being made, and the process being used usually determine which ferroalloy is used.

In ferromanganese making processes, the main components of manganese ore, $MnO_2$ and $Fe_2O_3$ are reacted with carbon in either a blast furnace or a submerged arc furnace (SAF). Currently, ferromanganese alloys are commonly produced in SAF using the carbothermal reduction method because a blast furnace is relatively energy inefficient

due to the large amount of manganese losses to slag. The reduction and smelting reactions can be represented by the following equations:

$$2\ MnO_2 + C = Mn_2O_3 + CO\ (g) \quad (2.1)$$

$$3\ Mn_2O_3 + C = 2\ Mn_3O_4 + CO\ (g) \quad (2.2)$$

$$Mn_3O_4 + C = 3\ MnO + CO\ (g) \quad (2.3)$$

$$MnO + C = Mn + CO\ (g) \quad (2.4)$$

$$7\ MnO + 10\ C = Mn_7C_3 + 7\ CO\ (g) \quad (2.5)$$

For reaction (2.4), the standard free energy ($\Delta G^o$) does not become negative until a temperature of 1400 $^oC$ is reached whereas it becomes negative from around 1250 $^oC$ for the reaction (2.5). This means that a low carbon ferromanganese cannot be produced without a considerable manganese loss into slag. The schematic diagram of a typical submerged arc furnace (SAF) process which produces three basic alloys: ferromanganese, silicomanganese, and ferromanganese-silicon, is shown in Figure 1 and specifications for these alloys are given in Table 2.[21] Figure 2 shows the equilibrium phases calculated by HSC thermodynamic software, which indicates the feasibility of carbon reduction reactions to produce manganese in thermal plasma.

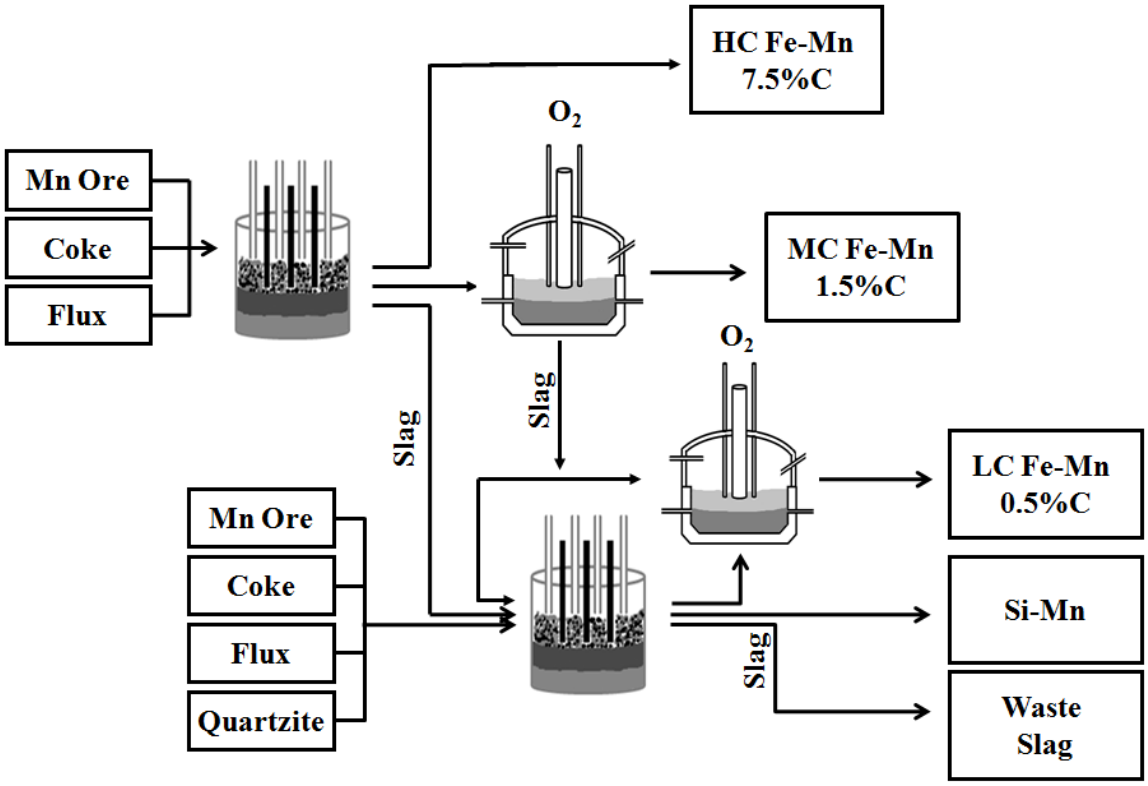


Figure 1. A schematic diagram of ferromanganese production

Table 2. Manganese alloy specification from ASTM 1998[21]

| Alloy | % Mn | % C (max) | % Si (max) | % P (max) | % S (max) |
|---|---|---|---|---|---|
| **Ferromanganese** | | | | | |
| Standard | | | | | |
| Grade A | 78-82 | 7.5 | 1.2 | 0.35 | 0.05 |
| Grade B | 76-78 | 7.5 | 1.2 | 0.35 | 0.05 |
| Grade C | 74-76 | 7.5 | 1.2 | 0.35 | 0.05 |
| Medium Carbon | | | | | |
| Grade A | 80-85 | 1.5 | 1.5 | 0.30 | 0.02 |
| Grade B | 80-85 | 1.5 | 1.0 | 0.30 | 0.02 |
| Grade C | 80-85 | 1.5 | 0.70 | 0.30 | 0.02 |
| Grade D | 80-85 | 1.5 | 0.35 | 0.30 | 0.02 |
| Nitrided medium carbon | 75-80 | 1.5 | 1.5 | 0.30 | 0.02 |
| Low-carbon | | | | | |
| Grade A | 85-90 | 0.75 | 2.0 | 0.20 | 0.02 |
| Grade B | 80-85 | 0.75 | 5.0-7.0 | 0.30 | 0.02 |
| **Silicomanganese** | | | | | |
| Grade A | 65-68 | 1.5 | 18.5-21.0 | 0.20 | 0.04 |
| Grade B | 65-68 | 2.0 | 16.0-18.5 | 0.20 | 0.04 |
| Grade C | 65-68 | 3.0 | 12.5-16.0 | 0.20 | 0.04 |
| **Fe-Mn Silicon** | 65-68 | 0.8 | 28.5-32.0 | 0.05 | 0.05 |

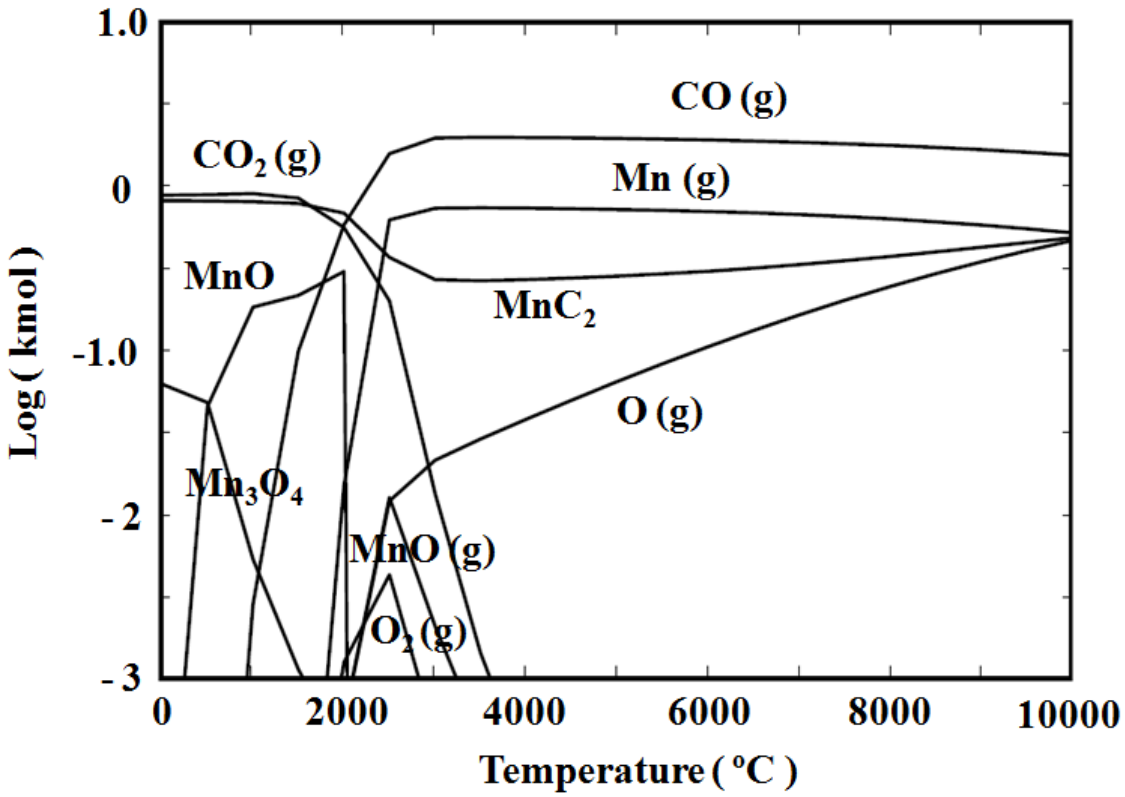


Figure 2. Feasibility of reduction reactions of manganese compounds by HSC [HSC chemistry, ver. 5.11, Outokumpu Research Oy, Pori, Finland, A. Roine]

## 2.2. Dephosphorization

Dephosphorization is one of the most important steps in the pretreatment of hot metal, the production of ferroalloys and stainless steels because phosphorus (P) can reduce the strength of steel and cause brittleness. Among the several P sources in the ferromanganese (Fe-Mn) making process, more than 80 % of P in the Fe-Mn alloy comes from the manganese ore, which usually contains around 0.2-0.6 % of phosphorus[22] and the rest comes from coke and lime. Because P is nobler than Mn and has a high affinity to Fe, almost all P is absorbed into Fe-Mn alloy in the form of $Fe_3P$ during the direct reduction by carbon in the smelting process.

The phosphorus in manganese ore takes the form of the ion $PO_4^{3-}$. The phosphorus materials found in manganese ores include kurskite $[Ca_3(PO_4)_2]_3{\cdot}Ca(CO_3) \cdot nH_2O$, francolite $[Ca_3(PO_4)_2]_3{\cdot}CaF_2{\cdot}nH_2O$, vivianite $Fe_3(PO_4)_2{\cdot}8H_2O$ and other phosphates.[23] Phosphorus can form several volatile compounds such as PO and $PO_2$ in an oxidizing atmosphere and as $P_2$, $P_4$, and PH in a reducing atmosphere. The dephosphorization methods commonly used in ferromanganese alloy industry and steel industry are as follows:

1) By using BaO or $BaCO_3$ under oxidizing conditions wherein the product is a phosphate as shown below:

$$1/2\ P_2 + 3/2(O^{2-}) + 5/4\ O_2 = PO_4^{3-} \qquad (2.6)$$

2) By using $CaC_2$, CaO and metal Ca under reducing conditions wherein phosphorus is removed as a phosphide as follows:

$$1/2\ P_2 + 3/2(O^{2-}) = P^{3-} + 3/4\ O_2 \quad (2.7)$$

The dephosphorization method under oxidizing conditions using BaO based fluxes may be represented as follows:

$$3/2\ BaO\ (s) + P + 5/2\ MnO\ (l) = 5/2\ Mn\ (l) + 1/2\ Ba_3(PO_4)_2\ (s) \quad (2.8)$$

The standard free energy ($\Delta G^o$) is -136713+89.3T J/mol,[24] which gives -23034 J/mol at 1000 ºC. The main problem in this process is the loss of manganese because manganese oxide is more stable than that of phosphorus at smelting temperatures.[25] Another problem of this process is temperature drop due to the decomposition of $BaCO_3$. Liu et al.[26] also successfully melted BaO-based flux and were able to remove phosphorus to the required level, but the time required to achieve this value was more than 30 minutes in a stagnant melt.[27-31]

The dephosphorization method under reducing conditions using metallic Ca-based fluxes may be represented as follows:

$$2\,[P] + 3Ca\,(l) = Ca_3P_2\,(s) \quad (2.9)$$

$\Delta G^o$ = -623457 + 118.19 T J/mol for this reaction.[32]

Carbon can be used to remove phosphorus from phosphates by the formation of gaseous phosphorus. The reactions can be given as follows:

$$Ca_3(PO_4)_2 + 5\,C = 3\,CaO + P_2\,(g) + 5\,CO\,(g) \quad (2.10)$$

$$Fe_3(PO_4)_2 + 8\,C = 3/2\,Fe_2P + 1/4\,P_2\,(g) + 8\,CO\,(g) \quad (2.11)$$

The environmental problem, however, is the main problem of the reduction process. The products of dephosphorization reaction under reducing conditions are phosphides ($Ca_3P_2$, $Fe_2P$, etc), which can produce toxic phosphine ($PH_3$) in contact with moisture by the following reaction: [33]

$$Ca_3P_2(s) + 6\,H_2O\,(l) = 3\,Ca(OH)_2\,(s) + 2\,PH_3(g) \quad (2.12)$$

Furthermore, the phosphine gas may form explosive mixtures with air and can ignite itself. When phosphine burns, it produces phosphorus pentoxide which is a severe respiratory irritant. When metallic Ca or Ba is used for the dephosphorization under

reducing conditions, the formation of $CaC_2$ or $BaC_2$ decreases the solubility of Ca or Ba in the metal.[34-37]

## 2.3. Plasma technology

Thermal plasma technology is associated with various applications such as spraying,[13,14] chemical vapor deposition, waste destruction, metallurgical refining,[17] and synthesis of fine powders in generating nanometer particles.[38-40] Plasma synthesis is carried out using a torch through which a high temperature plasma flame is formed. The high temperatures together with the high reactivity due to the presence of free ions and radicals make the plasma a powerful medium to promote high heat transfer rates and chemical reaction.[41] The raw materials fed into the plasma flame are reacted and evaporated while plasma forming gas provides an inert atmosphere and helps to prevent undesirable reactions.

There are several advantages of the thermal plasma system. First, chemical reactions are much faster than conventional processing because of the high temperature ($>10^4$ K). Second, quench rates of the product powders are very rapid to preserve the high-temperature phases.[42] Third, use of electricity as the primary energy source assures independence from the oxygen potential of the medium and, therefore, a controlled environment.[10-17, 43-45]

There are two types of high intensity arcs: 1) Direct Current (DC, nontransferred and transferred) and 2) Radio frequency (RF) arcs. In the case of DC arcs, both non-transferred and transferred arcs have been used to promote chemical reactions. Thus, DC plasma arc is more commonly used for material processing. The nontransferred arcs can

be operated in the low voltage range from 20 to 150 V, typically used at power levels below 100 kW, and plasma torches are used with tungsten cathode and copper anode.[46] The most commonly used plasma gases are Ar, He, $N_2$, $H_2$, and their mixtures. Oxidizing gases cannot be used for this plasma torch because tungsten cathode will be oxidized by these gases.

Hydrogen addition to the plasma gas has been reported to promote impurity removal.[17, 47] The gas flow rate is generally below 100 L/min, the energy densities in the hot gas may reach 145 MJ/$m^3$ and the plasma arc temperatures are between 6000 and 15,000 K.[48]

Transferred DC plasma torches are useful for the bulk heating of solids and melts.[49] Cathodes are constructed from either a water-cooled metal or more usually a refractory material that is consumed slowly by sublimation, e.g. graphite, tungsten, or molybdenum.

Anodes are made from metals with high thermal conductivities, such as copper or silver, and are usually in the form of flat ended cylinders to distribute the arc attachment.[50-52]

The gas flow rates are typically very low which can be important for controlling vapor phase reactions and condensation phenomena. The gas flow rate requirement is less than 200 L/min and energy densities may reach 2800 MJ/$m^3$.[48]

Transferred arc heaters typically operate at up to several thousand amperes (as high as 100,000 A with graphite electrodes) and a few hundred volts.[49] A schematic diagram of a (a) DC nontransferred and (b) transferred arc plasma torch is shown in Figure 3.[50]

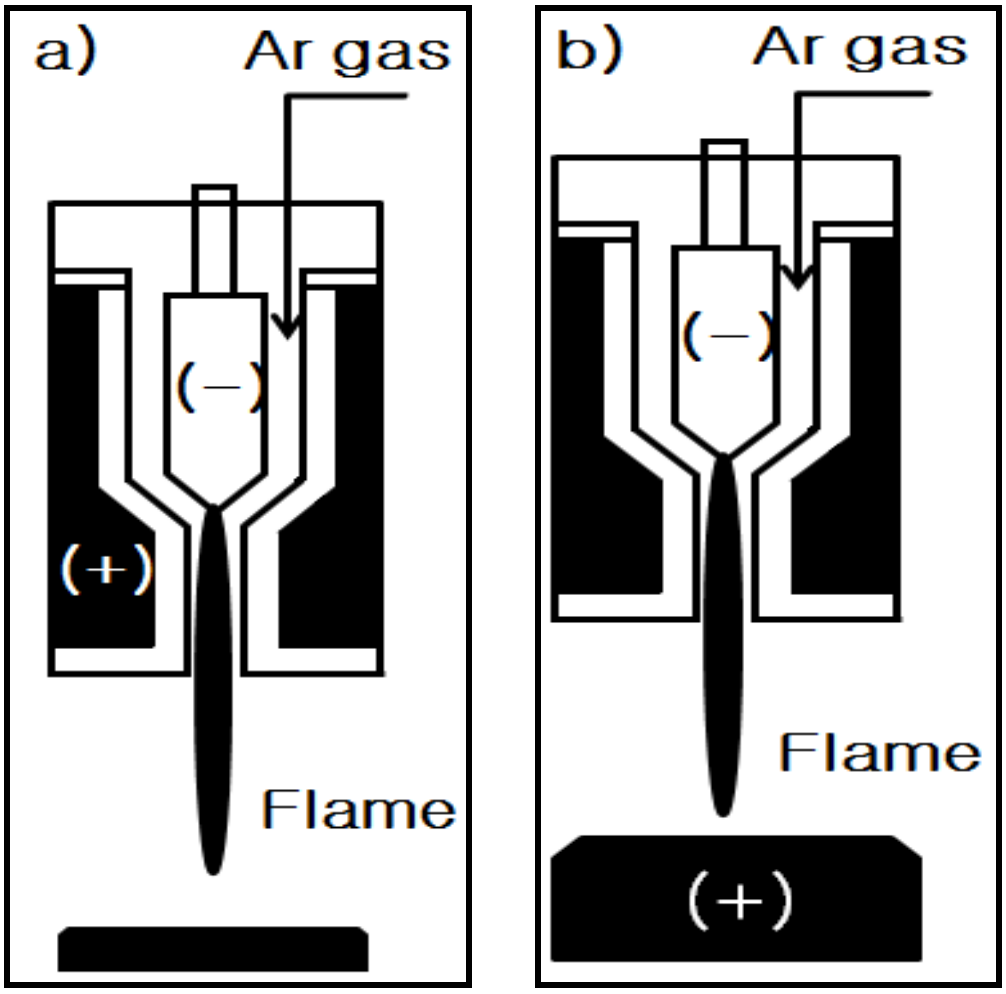


Figure 3. A schematic diagram of a DC arc plasma torch: (a) nontransferred arc, (b) transferred arc

## 2.4. Vaporization and thermal decomposition

During the smelting of manganese alloys, gaseous phosphorus can be formed according to reactions (2-10) and (2-11). An increase in operation temperature to boost the removal of phosphorus, however, will lead to excessive losses of manganese because of relatively high volatility of metal manganese. Although its boiling point is 2061 ºC, Mn has an appreciable vapor pressure at temperatures readily attainable in submerged arc

furnace (SAF); for example, the vapor pressure at 1600 ºC is 0.05 atm. Therefore, the removal of phosphorus before smelting is more desirable.

The thermal properties of the manganese, phosphorus, and their compounds are presented in Table 3. According to the table, the vaporizing removal of phosphorus directly from a manganese ore in which the phosphorus is in the form of phosphate, especially ferric phosphate, by its thermal decomposition may be possible. Although the exact decomposition temperatures of $Ca_3(PO_4)_2$ and $Fe_3(PO_4)_2$ are not available, their decomposition at the high temperatures provided by plasma flame can be expected.[53]

The thermal decomposition of the phosphates at a higher temperature than 1600 $^oC$ can be represented as the following reactions:

$$FePO_4 = 1/3\ Fe_3O_4 + 1/2\ P_2O_5\ (g) + 1/12\ O_2\ (g) \quad (2.13)$$

$$Fe_3(PO_4)_2 = Fe_3O_4 + 1/2\ P_2O_5\ (g) + PO\ (g) + 1/4\ O_2\ (g) \quad (2.14)$$

$$Ca_3(PO_4)_2 = 3\ CaO + P_2\ (g) + 2.5\ O_2\ (g) \quad (2.15)$$

In this high temperature, manganese high oxides such as $MnO_2$ and $Mn_2O_3$ also decompose to generate oxygen as follows:

$$MnO_2 = 1/2\ Mn_2O_3 + 1/4\ O_2\ (g) \quad (2.16)$$

$$Mn_2O_3 = 2/3\ Mn_3O_4 + 1/6\ O_2\ (g) \quad (2.17)$$

Table 3. Thermal properties of manganese, phosphorus and their oxides by HSC*

| | Melting Point (°C) | Boiling Point (°C) |
|---|---|---|
| Mn | 1246 | 2061 |
| $MnO_2$ | (Decomposes at 535°C) | - |
| $Mn_2O_3$ | (Decomposes at 940°C) | - |
| $Mn_3O_4$ | 1567<br>(Decomposes at 1700°C) | 2847 |
| MnO | 1945 | (3127) |
| P (White) | 44.2 | 280 |
| $P_4O_{10}$ | 340 | (Sublimation at 360°C) |
| $FePO_4$ | (Decomposes near 500°C) | - |
| $Fe_3(PO_4)_2$ | - | - |
| $Ca_3(PO_4)_2$ | 1670 | - |

* [A. Roine HSC chemistry, ver. 5.11, Outokumpu Research Oy, Pori, Finland]

It is noted that hematite ($Fe_2O_3$), the major form of iron contained in manganese ores, also decomposes to magnetite ($Fe_3O_4$), which is strongly magnetic, at the high temperatures. Figures 4 and 5 show the equilibrium phases calculated by HSC thermodynamic software, which indicates the feasibility of thermal decomposition of calcium phosphate and iron phosphate.

When thermal plasma is applied to heat manganese ore powder to high temperatures, the following effects are expected: 1) removal of phosphorus directly from manganese ores by the thermal decomposition of phosphates, 2) upgrading of manganese ores by the removal of the iron content in the ore using a simple magnetic separation. In addition, because of the high boiling points of $Mn_3O_4$ and MnO much higher than metallic Mn as can be seen in Table 3, the loss of manganese is expected to be low during the plasma application. The present study was initiated based on all these expectations.

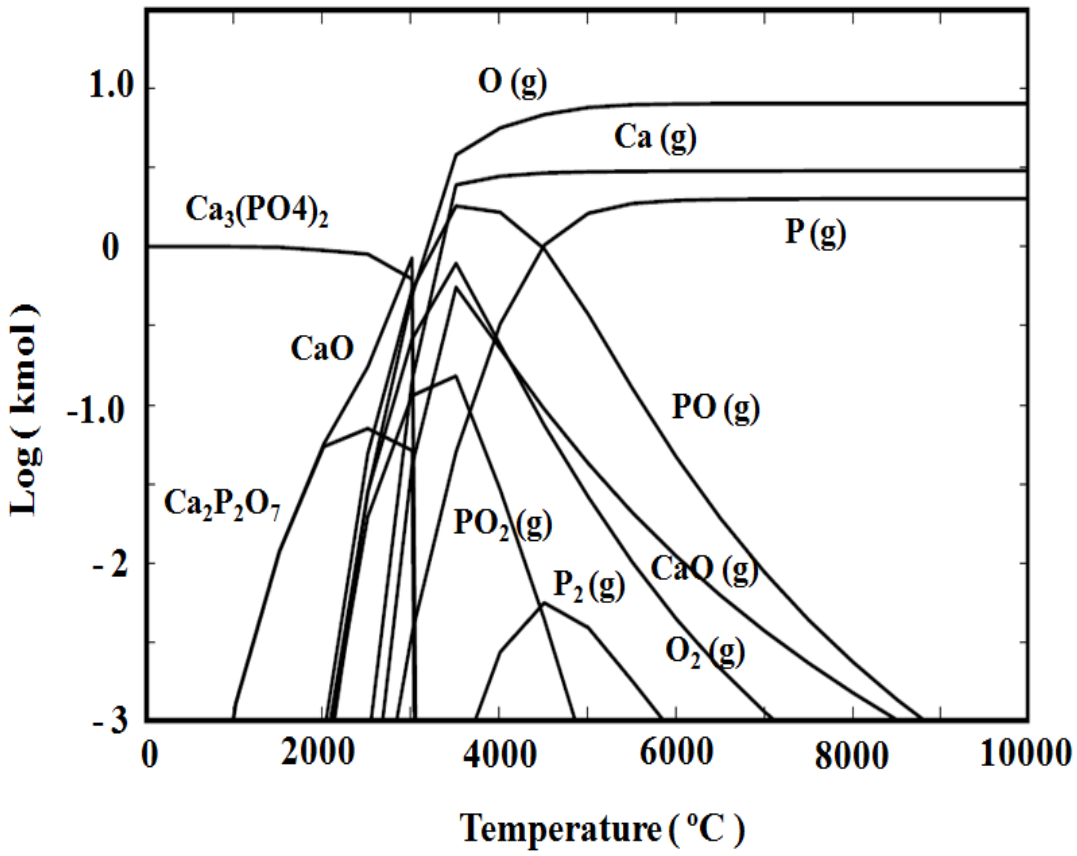


Figure 4. Feasibility of thermal decomposition of $Ca_3(PO_4)_2$ by HSC
[A. Roine HSC chemistry, ver. 5.11, Outokumpu Research Oy, Pori, Finland]

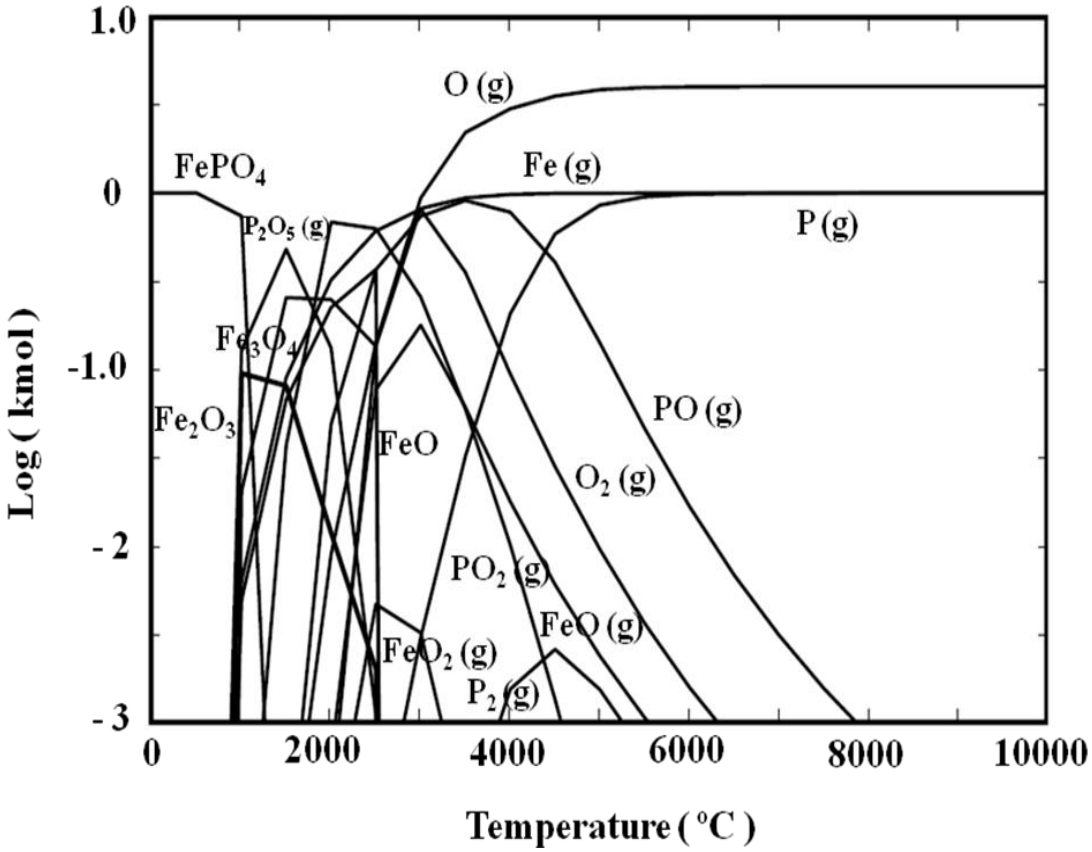


Figure 5. Feasibility of thermal decomposition of $FePO_4$ by HSC
[A. Roine HSC chemistry, ver. 5.11, Outokumpu Research Oy, Pori, Finland]

# 3. EXPERIMENTAL APPARATUSES AND PROCEDURES

## 3.1. Raw materials

In this study, two kinds of manganese ores (named H1 and LP) which were received from the Research Institute of Industrial Science and Technology (RIST), Korea, were used. Their chemical compositions are shown in Table 4. As can be seen in the table, their CaO contents are extremely low compared to their Fe contents. H1 ore of high manganese and phosphorus contents is used for the study for the removal of phosphorus, and LP ore of lower manganese and a higher iron contents than H1 ore is used for the study of the removal of iron by magnetic separation. The ore samples were crushed and ground until all particles were smaller than 100 μm, as required by the plasma system. In order to obtain necessary information about crystal phases, particle shape and thermal behavior of samples, X-ray diffraction (Siemens D-5000), Scanning Electron Microscopy (SEM, Topcon sm-300), and Thermogravity-Differential thermal analysis (TG-DTA) analyses were carried out.

Table 4. Chemical components of the manganese ore samples

| | T-Mn | T-Fe | P | Si | Al | Ca | Mg |
|---|---|---|---|---|---|---|---|
| H1 | 47.30 | 1.55 | 0.20 | 5.48 | 3.94 | 0.17 | 0.15 |
| LP | 42.91 | 2.38 | 0.17 | 11.75 | 3.98 | 0.12 | 0.10 |

### 3.2. Thermal plasma reactor system

Figure 6 shows the thermal plasma reactor system used in this study.[54] The system consists of a sample feeder (a), a plasma gun (b), a cylindrical reactor (c), a cooling chamber (d), a powder collector (e), and a scrubber (f). The sample feeder consisted of a sample container glass tube, a vibrator, and carrier gas lines. The sample, H1 or LP manganese ore, was fed toward the plasma flame with ultra high purity argon (99.99%) gas as a carrier gas. The plasma gun was designed by Praxair, CT. It consists of a water-cooled tungsten cathode and a copper anode. The maximum power is up to 80 kW. The plasma flame is generated between a tungsten cathode and a copper anode. The Ar gas was mainly used for making plasma flame. $H_2$ (99.9%) was added as a reducing agent or to enhance the flame of plasma.

The plasma gun was placed on the upside of the cylindrical reactor. The cylindrical reactor consisted of a water-cooled stainless steel tube and a graphite cylindrical tube placed inside the stainless steel tube. The inner diameter and length for the stainless steel tube are 15 cm and 60 cm, respectively. The graphite tube had an inner diameter of 7.6 cm and its length was the same as the stainless steel tube. Between the inner wall of the water-cooled stainless-steel tube and the graphite tube, graphite felt was placed to insulate the reactor. The cooling chamber which was made of a two-layer stainless-steel box was connected to the bottom of the cylindrical reactor and the temperature of the outgoing gas was kept lower than 150 ºC by using cooling water. The powder collecting system contained two stainless collectors. One is for the collecting of the final product and the other is for the bypass of the off-gas. To collect the final product, a teflon coated polyester filter with a pore size of 1 μm was used.

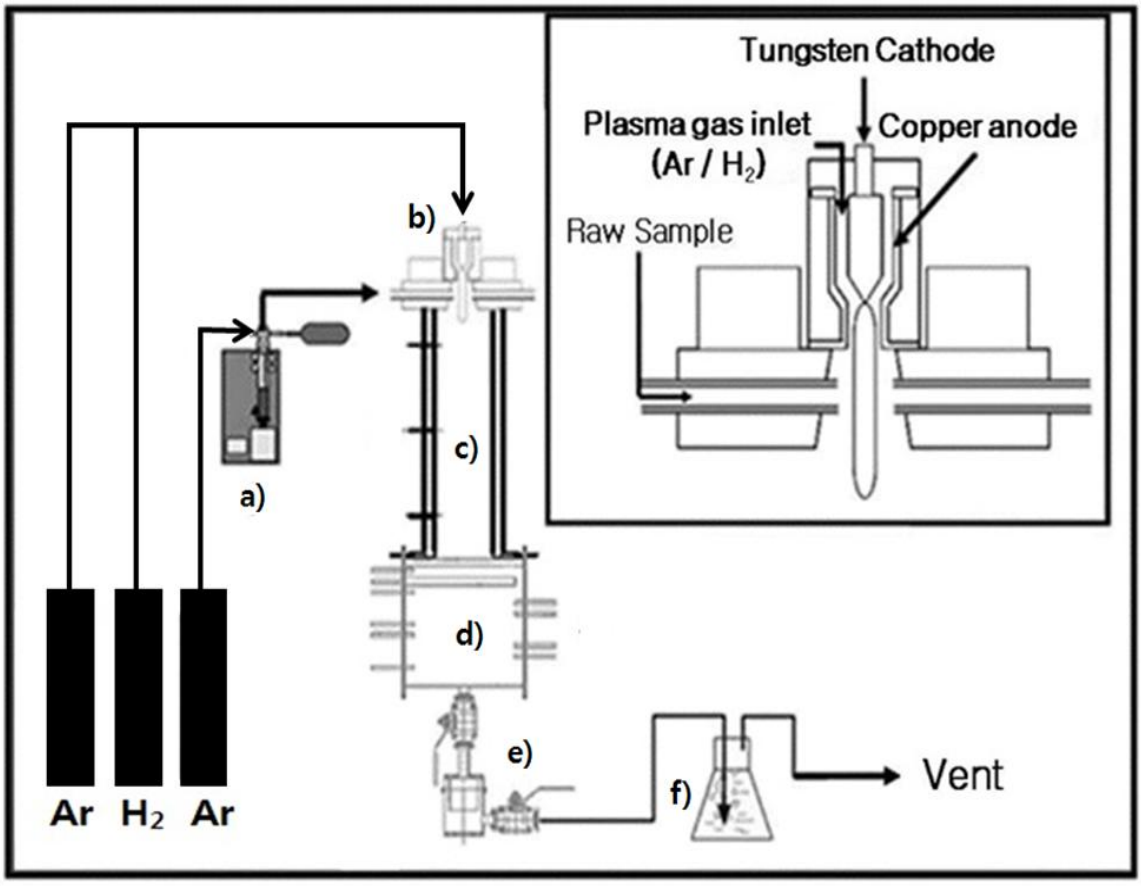


Figure 6. A schematic diagram of the plasma reactor system: a) sample feeder, b) plasma gun, c) cylindrical reactor, d) cooling chamber, e) powder collector, f) scrubber
[Adapted from Ref. 54]
[Plasma spray gun, Praxair. Inc, CT, Model SG-100, nominal power rating 80 kW]

The off gases passed through the scrubber which was used for removal of uncollected powder and for prevention of the back flow of the off-gas. Finally, the off-gas was exhausted through the fume hood system.

To start the experiment, the reactor was purged in advance with Ar gas at 20 L/min based on the ambient temperature and pressure (25 ºC and 86.1 kPa). After the experiment, the reactor was also purged with Ar gas at the same condition. Afterward, the powder collector was disassembled from the reactor system. The collected final product on the filter was stored in a plastic zip bag for further analyses.

In this system, when the injected raw ore powder passes through the plasma flame, the volatile component in the ore is vaporized and removed from the ore and collected in the filter of the powder collector (Figure 6e) together with elutriated dust after being condensed. This condensed dust will be called the filtered product from here on. Therefore, the refined ore remained in the cooling chamber of the reactor (Figure 6d). This remained particle will be called the reactor product from here on.

### 3.3. Reproducibility test

Because of the complex reaction system involving plasma and the use of natural ore, there is considerable scatter in the data. Also, the amount of phosphorus in the raw manganese ore is quite small and phosphorus analysis by ICP is difficult. Thus, some extent of data scattering was inevitable in this study. To evaluate the reproducibility of the experimental results, the following experiment was carried out three times under the same conditions; the torch power was 14.9 kW; the Ar gas flow rate was 28.1 L/min (25 ºC and 86.1 kPa); the powder feeding rate was 1.14 g/min; the carrier gas flow rate was

3.15 L/min (25 ºC and 86.1 kPa). Each sample was analyzed by ICP. The experimental results are given in Table 5. This degree of uncertainty is indicated also in Figure 7.

### 3.4. Product characterization

The samples, before and after experiments, were analyzed using analytical scanning electron microscopy (SEM, Topcon sm-300) equipped with energy dispersive X-ray spectrometry (EDS) which can determine the distribution of component elements. Inductively Coupled Plasma (ICP) analysis was used for the chemical analyses of manganese, iron, and phosphorus contents in the product samples. To analyze the thermal behavior of the raw sample, a Thermogravity-Differential Thermal Analysis (TG-DTA) system was used. Temperature range was from 25 to 1100ºC for the TG-DTA analysis. The information about the phase transformations of the manganese oxides and other components was obtained by analyzing XRD patterns (Siemens D-5000). The XRD was carried out using Cu-Kα radiation with wavelength of 1.542Å. The scan angle (2 $\theta$) ranged from 20º to 100º.

Table 5. P, Mn wt% and P/Mn ratio for reproducibility test: 14.9 kW of torch power, 28.1 L/min of Ar gas flow rate, 1.14 g/min of feeding rate, and 3.15 L/min of carrier gas at 25 ºC and 86.1 kPa

| The number of experiment | Filter | | | Reactor | | |
|---|---|---|---|---|---|---|
| | P (wt%) | Mn (wt%) | P/Mn | P (wt%) | Mn (wt%) | P/Mn |
| # 1 | 0.22 | 52.6 | 0.00418 | 0.083 | 58.5 | 0.00142 |
| # 2 | 0.25 | 49.3 | 0.00507 | 0.080 | 53.6 | 0.00149 |
| # 3 | 0.26 | 49.3 | 0.00527 | 0.074 | 53.8 | 0.00137 |

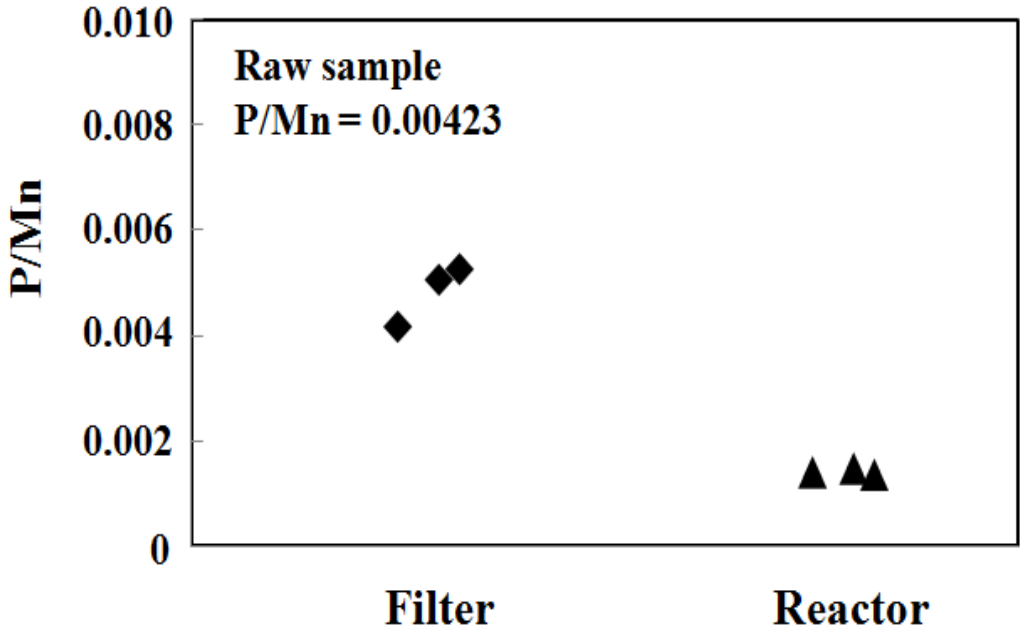


Figure 7. P/Mn ratio for the reproducibility test: 14.9 kW of torch power, 28.1 L/min of Ar gas flow rate, 1.14 g/min of feeding rate, and 3.15 L/min of carrier gas at 25 ºC and 86.1 kPa

# 4. EXPERIMENTAL RESULTS AND DISCUSSION

## 4.1. Direct removal of phosphorus by plasma treatment

### 4.1.1. Properties of H1 ore

In order to investigate the properties of the H1 raw sample, analyses by XRD, SEM, and TG-DTA were performed, and the results are shown in Figures 8~10. The XRD results indicate that the main crystal components in the raw ore H1 are $MnO_2$ (JCPDS 44-0141) and $SiO_2$ (JCPDS 87-0703). $Al_2Si_2O_5(OH)_4$ (JCPDS 14-0164) and $Fe_2O_3$ (JCPDS 87-1166) phases were also observed. Figure 9 shows the morphologies of the as-received H1 raw sample. The H1 raw sample has an irregular shape and the particle size is less than 100 μm. According to the TG-DTA analysis result, moisture was first removed at around 100 ºC. Secondly, $MnO_2$, the major component of the ore, was decomposed to $Mn_2O_3$ at around 400 ºC. Dehydration reaction of the $Al_2Si_2O_5(OH)_4$ phase occurred at around 500 ºC. Finally, the $Mn_2O_3$ phase decomposed to $Mn_3O_4$ at around 900 ºC.

### 4.1.2. Feasibility of the plasma treatment

To investigate the feasibility of plasma application for the dephosphorization of manganese ores, a series of experiments were carried out using Ar and $Ar/H_2$ mixture gases. The test conditions are listed in Table 6. Firstly, the experiment was carried out with pure Ar gas as the plasma gas to investigate the decomposition of the phosphorus

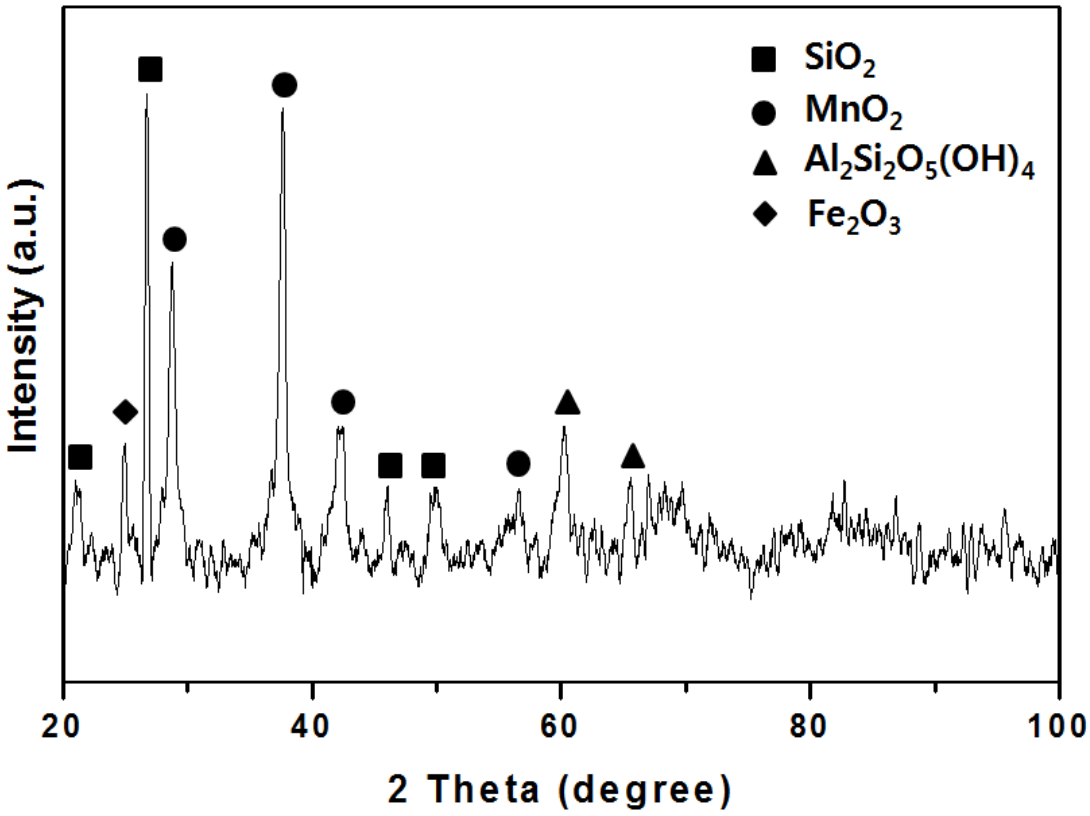


Figure 8. XRD patterns of the H1 raw sample

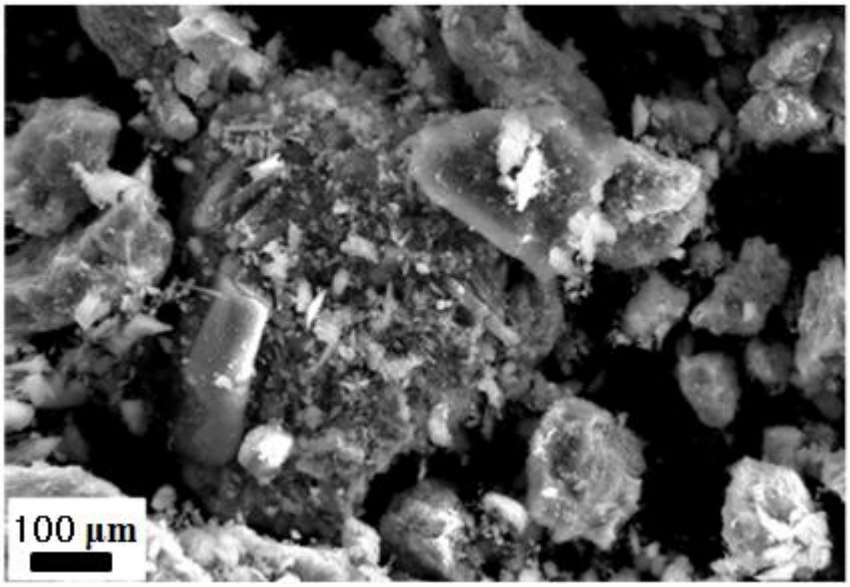


Figure 9. SEM micrograph of the H1 raw sample

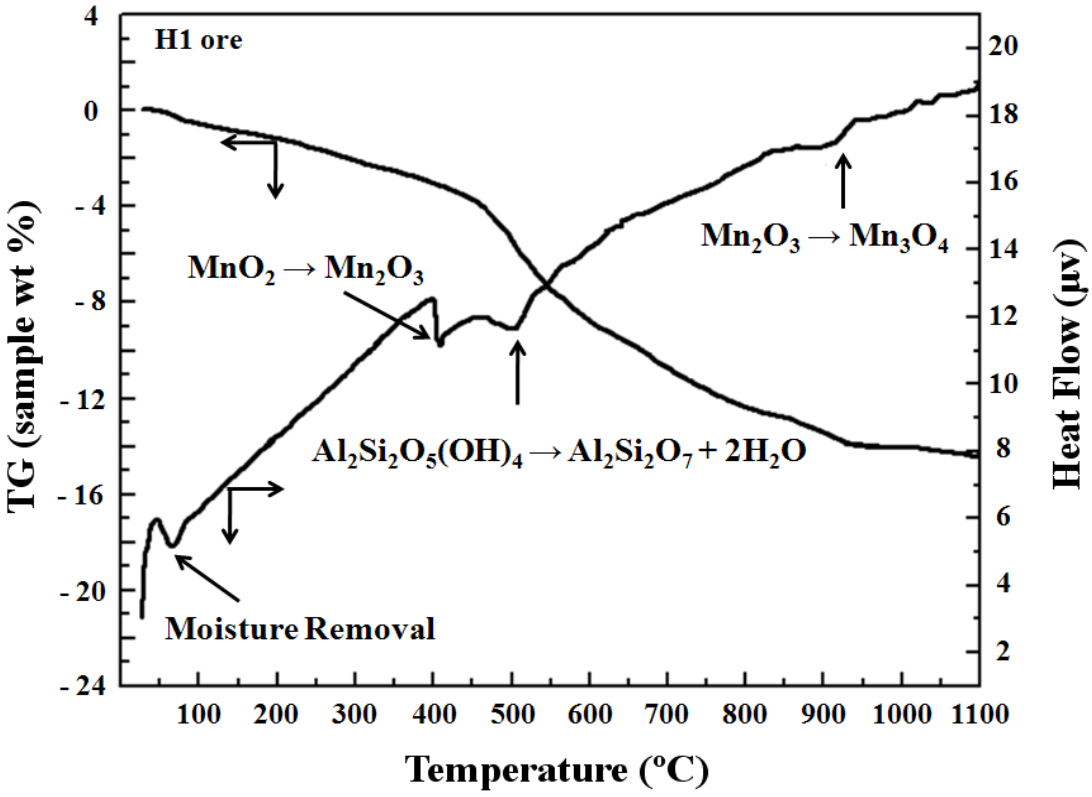


Figure 10. TG-DTA analysis of the H1 raw sample (Heating rate 5°C/min)

Table 6. Experimental conditions for the feasibility test

| kW | Ar (L/min) | $H_2$ (L/min) | Feed rate (g/min) | Carrier gas (L/min) |
|---|---|---|---|---|
| 5.9 | 28.08 | 0 | 2.25 | 2.1 |
| 6.78 | 28.08 | 0.67 | 2.22 | 2.1 |

compound in the manganese ore. To improve the volatility of the phosphorus compound, hydrogen gas was added as a reductant in the second experiment. After the experiments, qualitive and quantitative analyses of phosphorus in the products were performed using SEM, EDS, and ICP. The phase transformation of the main components in ore sample was analyzed by XRD patterns.

Figure 11 shows the XRD patterns after plasma treatment with Ar gas, indicating that the $MnO_2$ phase transformed to $Mn_2O_3$ (JCPDS 24-0508), $Mn_3O_4$ (JCPDS 24-0734), and MnO (JCPDS 07-0230). The thermal decomposition of the manganese oxides can be expected from Table 3 and Figure 10, which indicate that $MnO_2$ was transformed to $Mn_2O_3$, $Mn_3O_4$, and MnO at 535ºC, 940ºC, and 1700 ºC, respectively. Thus, the present plasma system provides enough temperature for the decomposition of manganese ore. The major phase of the raw sample is $MnO_2$ and $SiO_2$ phases, as shown in Figure 11 a). Figure 11 b) is the XRD pattern of the filtered product collected from the filter after plasma treatment, which shows that the $MnO_2$ phase transformed to $Mn_3O_4$ and MnO and $SiO_2$ phase still remained.

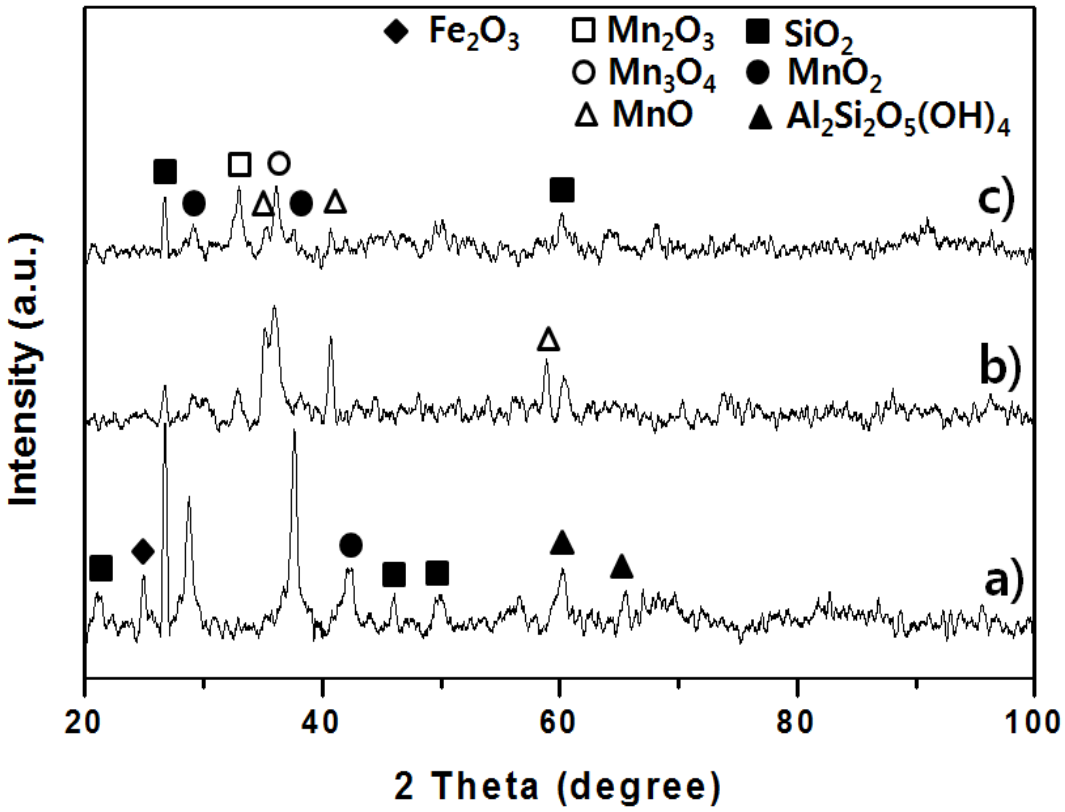


Figure 11. XRD patterns after plasma treatment with Ar gas for feasibility test: a) H1 raw sample, b) filtered product, and c) reactor product

Figure 11 c) is that of the reactor product collected from the cooling chamber after plasma treatment, which illustrates that the major phases are $Mn_2O_3$ and $Mn_3O_4$ and unreacted $MnO_2$ was still observed. The latter is thought to be caused by an uneven distribution of feed in the plasma. Figure 12 shows the SEM micrograph of the plasma treated samples, both collected from the filter (Figure 12a) and from the reactor (Figure 12b). According to the SEM micrograph, the shape was changed from irregular shape to spherical shape in case of the filtered product. This means that elutriated dust was fully melted and then solidified or that volatile components were vaporized and then condensed. This verifies that the plasma system provides enough heat so that even MnO particles of very high melting point can melt during the treatment.

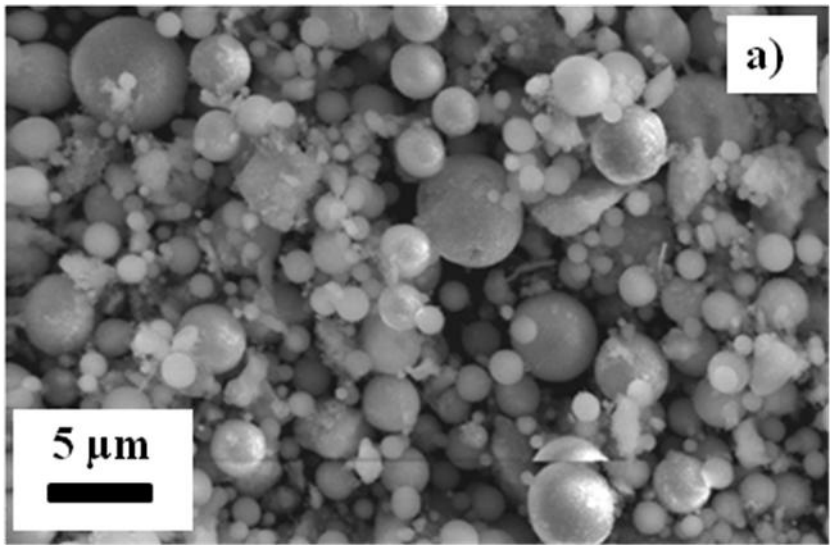


a)

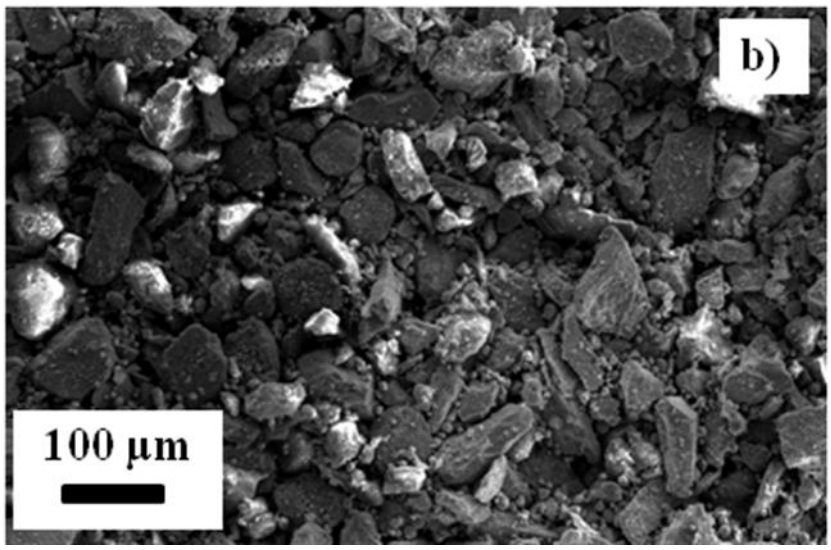


b)

Figure 12. SEM micrograph after plasma treatment with Ar gas for feasibility test: a) filtered product and b) reactor product

Figure 13 shows the XRD patterns of this sample after plasma treatment with $Ar/H_2$ gases. Almost the same trends as with just argon were observed, but all $MnO_2$ was transformed to MnO in the filtered product, as can be seen in Figure 13 b). In the reactor product, Figure 13 c), the major phases are $Mn_3O_4$ and MnO. The $SiO_2$ phase was also observed in both products. Figure 14 shows the SEM micrograph after plasma treatment with $Ar/H_2$ gases. The general aspects are quite similar to those observed with just Ar gas, but more spherical particles were observed in the reactor product. The latter can be ascribed to an increase of the flame temperature with the addition of hydrogen gas in the plasma gas.

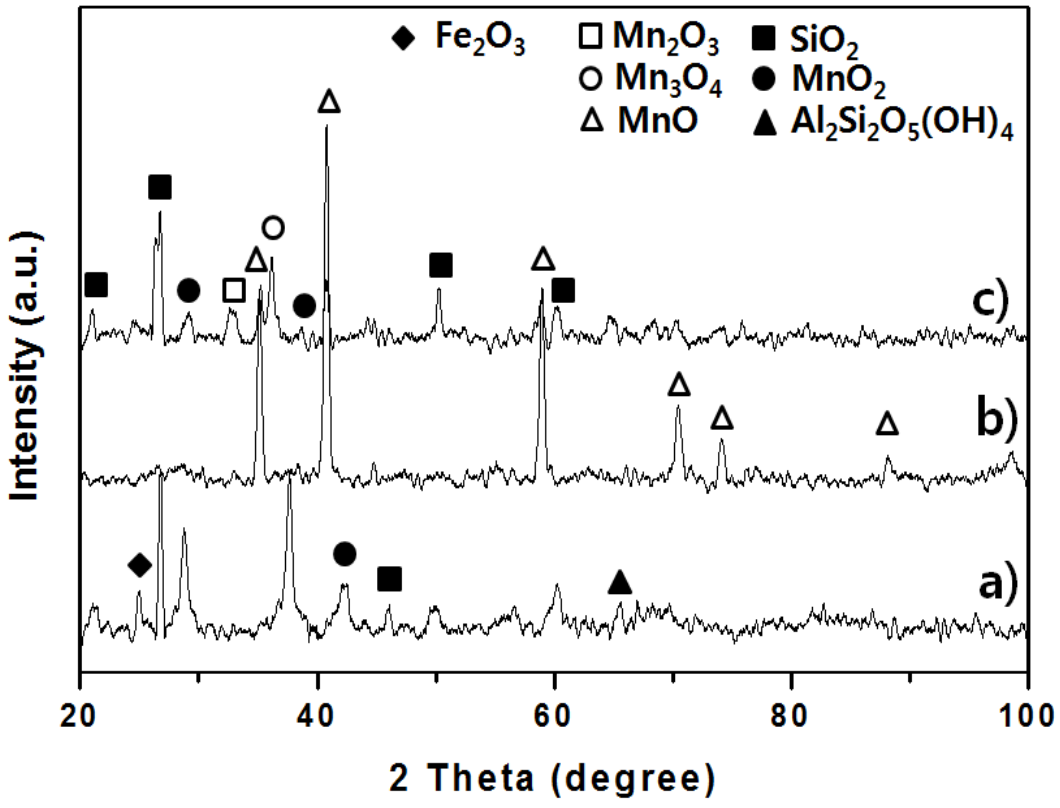


Figure 13. XRD patterns after plasma treatment with $Ar/H_2$ gases for feasibility test: a) H1 raw sample, b) filtered product, and c) reactor product

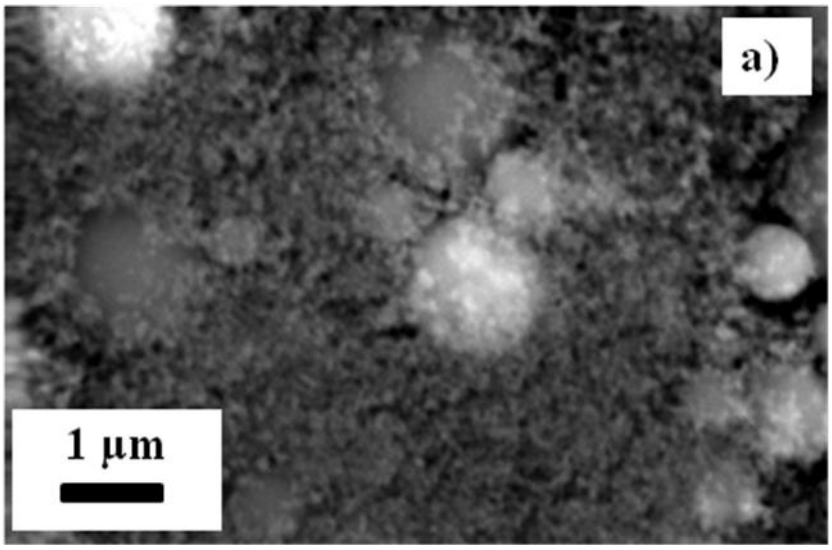


a)

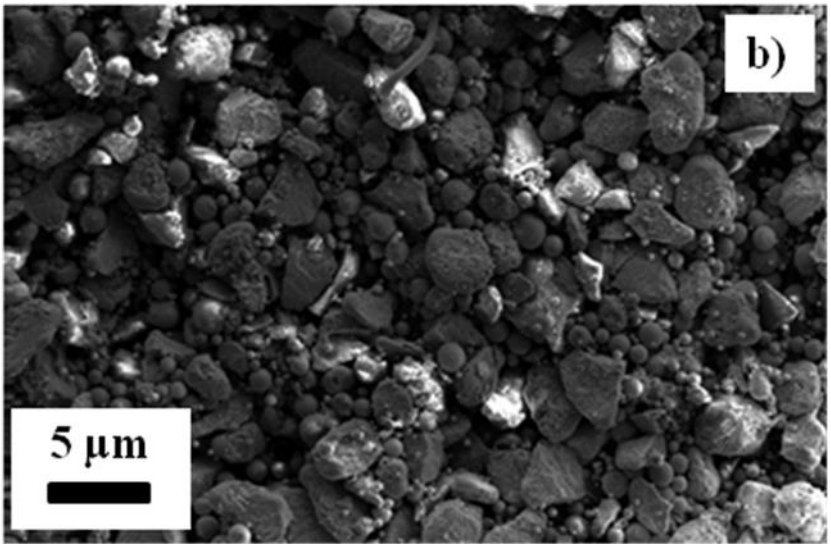


b)

Figure 14. SEM micrograph after plasma treatment with $Ar/H_2$ gases for feasibility test: a) filtered product and b) reactor product

The feasibility of plasma treatment for the direct removal of phosphorus from the manganese ore is evaluated from the experimental results given in Table 7 and Figure 15, which include the phosphorus wt%, the manganese wt%, and the P/Mn ratio in both the filter and the reactor product. The P/Mn ratio is the relevant factor in the determination of dephosphorization degree, because the plasma treatment reduces the weight of the solid by thermal decomposition. The P/Mn ratio will not change if the P and Mn are not vaporized. The ratio will decrease if P is selectively vaporized (removed) from the ore. The initial P/Mn ratio in the raw H1 ore is 0.00423. From the experiment results, Table 7 and Figure 15, it can be seen that when the plasma treatment was applied to the manganese ore, the P/Mn ratios in the filtered product were much higher than those in the reactor product, and the P/Mn ratios in the reactor product were lower than those in the raw ore. Especially when hydrogen is added to the plasma gas, the P/Mn ratio in the filtered product was 3 times higher than that in the reactor product. This is because the hydrogen reduced the phosphates or phosphorus oxides in the ore into phosphorus gases such as P, $P_2$, and $PH_3$, the vapor pressures of which are much higher than those of the phosphates or phosphorus oxides. Therefore, it can be concluded that the application of plasma for the removal of phosphorus directly from the raw manganese ores is feasible, especially when hydrogen is added to the plasma gas as a reductant. It is noted that because the amount of phosphorus in the raw manganese ore is quite small and technical difficulties in the chemical analysis of phosphorus by ICP, some data scattering was inevitable in this study. In addition, when hydrogen was used, the torch power increased (this was designed by the maker to secure a stable plasma flame), which led to a higher temperature of plasma flame. This temperature may have increased the dephosphorization.

Table 7. P, Mn wt%, P/Mn ratio for feasibility tests using Ar (28.1 L/min) and Ar/$H_2$ (28.1 / 0.67 L/min) gases at 25 ºC and 86.1 kPa

| | Filter | | | Reactor | | | |
|---|---|---|---|---|---|---|---|
| | P (wt%) | Mn (wt%) | P/Mn | P (wt%) | Mn (wt%) | P/Mn | % P removal |
| Raw Sample | 0.200 | 47.3 | 0.00423 | 0.200 | 47.3 | 0.00423 | - |
| Ar (5.9 kW) | 0.100 | 55.3 | 0.00186 | 0.063 | 56.3 | 0.00112 | 68.5 |
| Ar / $H_2$ (6.78kW) | 0.200 | 55.0 | 0.00363 | 0.075 | 60.4 | 0.00124 | 62.5 |

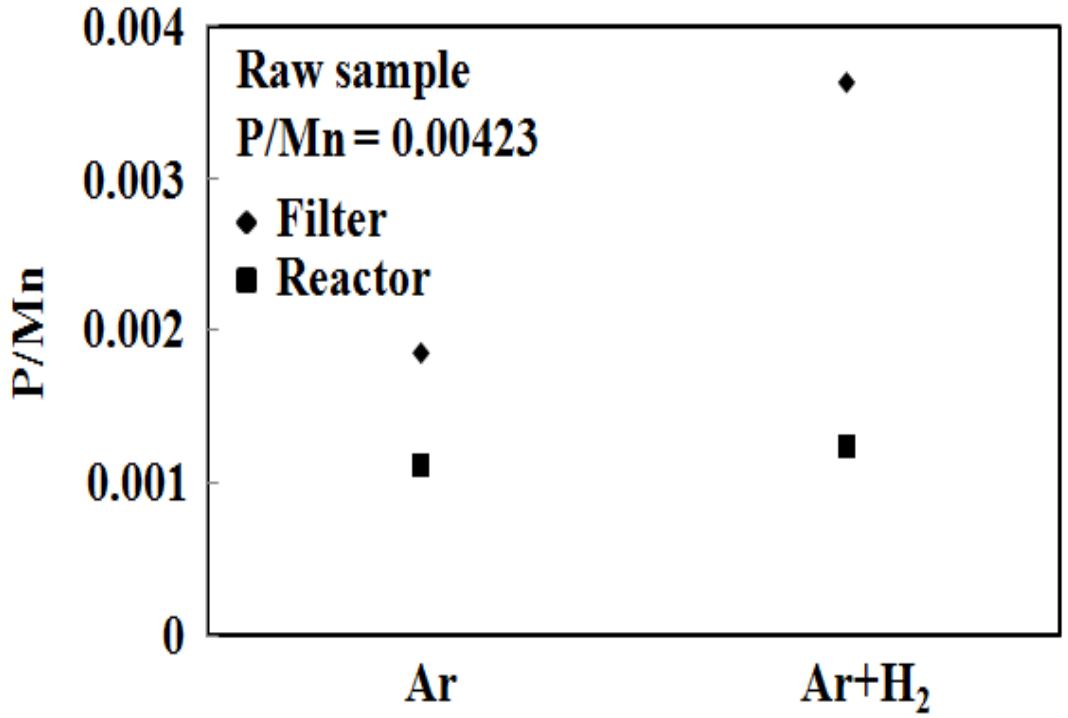


Figure 15. P/Mn ratio for the feasibility test by using Ar (28.1 L/min) and Ar/$H_2$ (28.1 / 0.67 L/min) gases at 25 ºC and 86.1 kPa

As the overall results for the feasibility test, when only Ar gas is used as the plasma gas, about 68.5 % of the P was removed and Mn wt% was increased to 56.3. When hydrogen gas is added, about 62.5 % the P was removed and wt % of Mn was increased to 60.4 from the reactor product.

### 4.1.3. Effect of the Ar gas flow rate

To investigate the effect of the Ar gas flow rate as a primary gas, the experiments were carried out at three different Ar gas flow rates, 21.4, 28.1 and 34.8 L/min (25 ºC and 86.1 kPa). The experimental conditions are shown in Table 8, and the experimental results are given in Table 9 and Figure 16. As can be seen, when the argon gas flow rate was increased, the P/Mn ratio in the filtered product decreased while that in the reactor product rather increased. This may be ascribed to the shorter residence time and the lower plasma flame temperature with the increase of the flow rate of argon gas. The flow rate of argon gas, therefore, should be kept as minimum as possible.

Table 8. Experimental conditions for the effect of Ar gas flow rate: 21.4, 28.1, and 34.8 L/min at 25 ºC and 86.1 kPa

| Torch power ( kW ) | Ar gas Flow Rate (L/min) | $H_2$ gas Flow Rate (L/min) | Powder Feed Rate (g/min) | Carrier gas Flow Rate (L/min) |
|---|---|---|---|---|
| 5.9 | 21.4 | - | 2.14 | 2.1 |
| 5.9 | 28.1 | - | 2.25 | 2.1 |
| 5.9 | 34.8 | - | 2.14 | 2.1 |

Table 9. P, Mn wt%, and P/Mn ratio at various Ar gas flow rates: 21.4, 28.1, and 34.8 L/min at 25 ºC and 86.1 kPa

| | Filter | | | Reactor | | | |
|---|---|---|---|---|---|---|---|
| | P (wt%) | Mn (wt%) | P/Mn | P (wt%) | Mn (wt%) | P/Mn | % P removal |
| Ar 21.4 L/min | 0.142 | 53.0 | 0.00268 | 0.057 | 59.9 | 0.00095 | 71.5 |
| Ar 28.1 L/min | 0.103 | 55.3 | 0.00186 | 0.063 | 56.3 | 0.00112 | 68.5 |
| Ar 34.8 L/min | 0.110 | 55.0 | 0.00200 | 0.060 | 58.6 | 0.00102 | 70.0 |

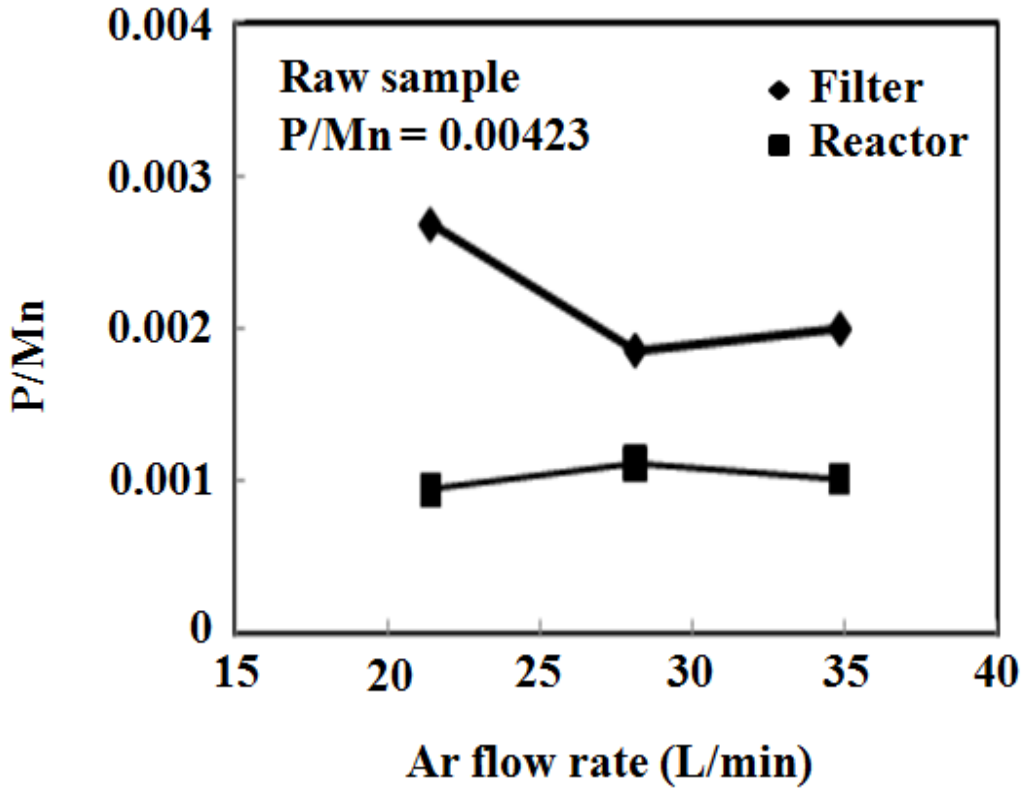


Figure 16. P/Mn ratio of the final product obtained from filter and reactor at various Ar gas flow rate: 21.4, 28.1, and 34.8 L/min at 25 ºC and 86.1 kPa

4.1.4. Effect of the $H_2$ gas flow rate

To evaluate the effect of the $H_2$ concentration in the plasma gas, the experiment was also conducted with increasing $H_2$ gas flow rate from 0 to 0.67 L/min. The experimental conditions are shown in Table 10, and the experimental results are presented in Table 11 and Figure 17. The addition of hydrogen to the plasma gas clearly showed a positive effect on the dephosphorization, but there was an optimum point. When the hydrogen gas is used, iron oxides in the ore can also be reduced to metallic Fe, which has such a strong affinity with phosphorus that iron phosphide ($Fe_2P$) can be formed. This formation of iron phosphide is a possible reason for the optimum hydrogen content. In this experiment, the optimum $H_2$ flow rate was found to be 0.1 L/min at 28.08 L/min of Ar gas flow rate. It is noted that the use of hydrogen can cause the formation of toxic phosphene ($PH_3$), although the generated amount of phosphene during the plasma treatment is expected to be small.

Table 10. Experimental conditions for the effect of hydrogen gas flow rate: 0, 0.06, and 0.67 L/min at 25 ºC and 86.1 kPa

| Torch power ( kW ) | Ar gas Flow Rate (L/min) | $H_2$ gas Flow Rate (L/min) | Powder Feed Rate (g/min) | Carrier gas Flow Rate (L/min) |
|---|---|---|---|---|
| 5.9 | 28.1 | 0 | 2.25 | 2.1 |
| 6.3 | 28.1 | 0.06 | 2.10 | 2.1 |
| 6.78 | 28.1 | 0.67 | 2.22 | 2.1 |

Table 11. P, Mn wt% and P/Mn ratio at various hydrogen gas flow rates: 0, 0.06, and 0.67 L/min at 25 ºC and 86.1 kPa

| | Filter | | | Reactor | | | |
|---|---|---|---|---|---|---|---|
| | P (wt%) | Mn (wt%) | P/Mn | P (wt%) | Mn (wt%) | P/Mn | % P removal |
| $H_2$ 0 L/min | 0.120 | 55.3 | 0.00217 | 0.100 | 56.3 | 0.00178 | 50.0 |
| $H_2$ 0.06 L/min | 0.180 | 55.1 | 0.00326 | 0.090 | 56.2 | 0.00160 | 55.0 |
| $H_2$ 0.67 L/min | 0.200 | 55.0 | 0.00363 | 0.075 | 60.4 | 0.00124 | 62.5 |

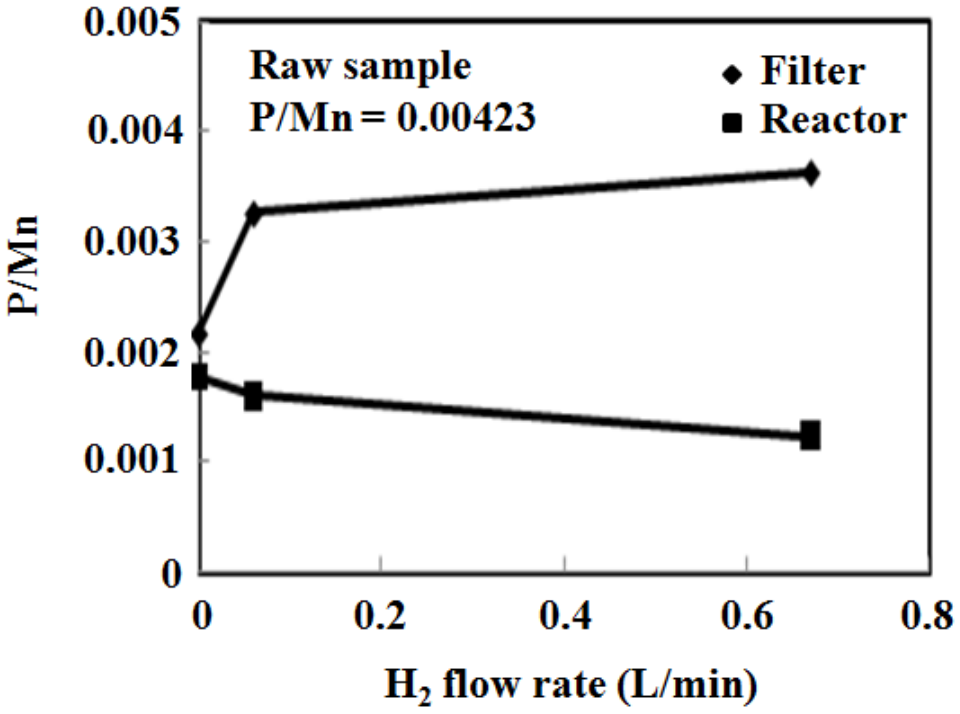


Figure 17. P/Mn ratio of the final product obtained from filter and reactor at various hydrogen gas flow rates: 0, 0.06, and 0.67 L/min at 25 ºC and 86.1 kPa

4.1.5. Effect of the plasma torch power

To evaluate the effect of the plasma torch power that is related to flame temperature, dephosphorization experiments were carried out by varying the torch power from 5.9 to 14.9 kW. The experimental conditions are shown in Table 12, and the experimental results are presented in Table 13 and Figure 18. As expected, dephosphorization clearly increased with an increase in the torch power without any significant loss of manganese to the off-gas (and dust). It may be concluded that an increase of torch power is more effective for the improvement of the dephosphorization by plasma treatment than an increased $H_2$ content in the plasma gas considering $PH_3$ generation. Based on Table 2, when the phosphorus content in the manganese ore is below 0.2%, it can make all grades of ferromanganese alloy in terms of phosphorus. During the plasma treatment in this work, P was decreased from 0.2% in the raw material to 0.057 wt% in the recovered product.

Table 12. Experimental conditions for the effect of torch powers: 5.9, 8.5, 11.8, and 14.9 kW at 25 ºC and 86.1 kPa

| Torch power ( kW ) | Ar gas Flow Rate (L/min) | $H_2$ gas Flow Rate (L/min) | Powder Feed Rate (g/min) | Carrier gas Flow Rate (L/min) |
|---|---|---|---|---|
| 5.9 | 28.1 | - | 1.19 | 3.15 |
| 8.5 | 28.1 | - | 1.14 | 3.15 |
| 11.8 | 28.1 | - | 1.17 | 3.15 |
| 14.9 | 28.1 | - | 1.14 | 3.15 |

Table 13. P, Mn wt% and P/Mn ratio at various torch powers: 5.9, 8.5, 11.8, and 14.9 kW at 25 ºC and 86.1 kPa

| | Filter | | | Reactor | | | |
|---|---|---|---|---|---|---|---|
| | P (wt%) | Mn (wt%) | P/Mn | P (wt%) | Mn (wt%) | P/Mn | % P Removal |
| 5.9 kW | 0.150 | 53.6 | 0.00280 | 0.110 | 57.2 | 0.00192 | 45.0 |
| 8.5 kW | 0.210 | 52.8 | 0.00398 | 0.100 | 58.2 | 0.00172 | 50.0 |
| 11.8 kW | 0.200 | 51.3 | 0.00390 | 0.090 | 58.6 | 0.00154 | 55.0 |
| 14.9 kW | 0.220 | 52.6 | 0.00418 | 0.083 | 58.5 | 0.00142 | 58.5 |

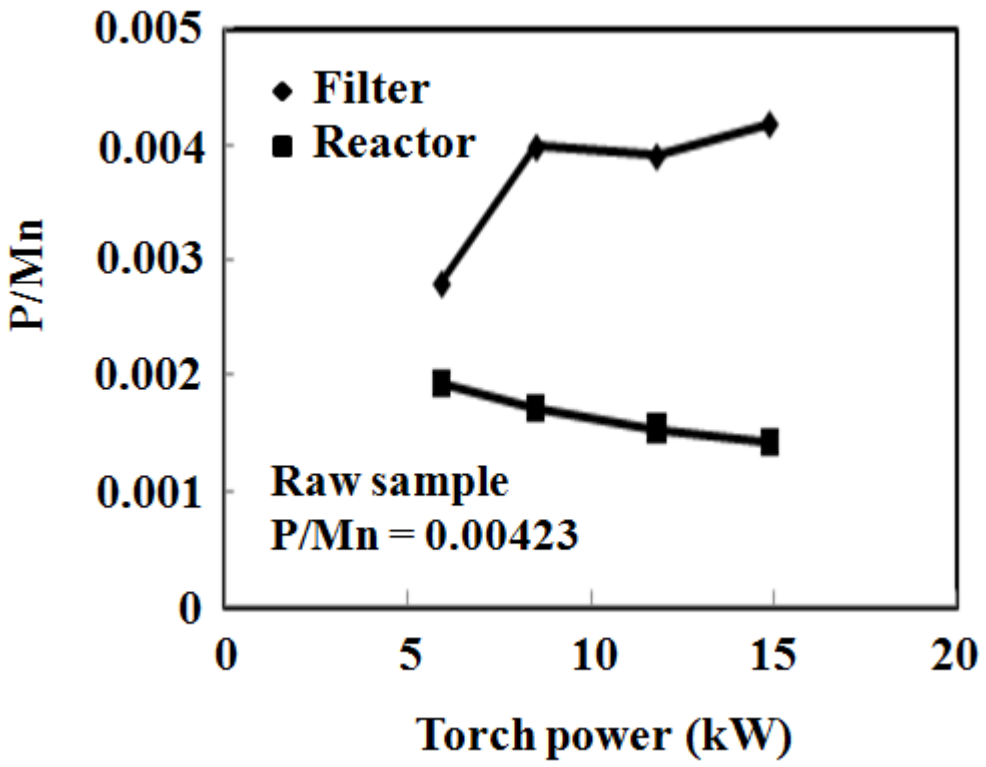


Figure 18. P/Mn ratio of the final product obtained from filter and reactor at various torch powers: 5.9, 8.5, 11.8, and 14.9 kW at 25 ºC and 86.1 kPa

## 4.2. Upgrading of a manganese ore by plasma treatment

### 4.2.1. Properties of LP ore

In the study on the upgrading of a manganese ore by plasma treatment, LP manganese ore which is a low grade and higher iron content manganese ore than H1 ore was used. Before the main test, the properties of the LP raw sample were investigated using the same procedure as used for the H1 ore sample. The results of XRD, SEM, and TG-DTA analyses are shown in Figures 19 ~ 21. The general properties of the LP ore sample were found to be very similar to those of the H1 sample, as can be expected from their similar chemical compositions. The XRD result indicates that the main crystal components in the LP raw ore are $MnO_2$ (JCPDS 44-0141) and $SiO_2$ (JCPDS 87-0703). $Fe_2O_3$ (JCPDS 87-1166) phase was also observed. Figure 20 shows the morphology of the as-received LP raw sample. The LP raw sample has an irregular shape like the H1 ore and the particle size is less than 100 μm. According to the TG-DTA analysis result, moisture was firstly removed at around 100 ºC. Secondly, $MnO_2$, the major component of the ore, was decomposed to $Mn_2O_3$ at around 400 ºC. The decomposition of $Mn_2O_3$ to $Mn_3O_4$ at around 900 ºC is not clearly shown.

### 4.2.2. Magnetic separation

As mentioned before, this part of the study is based on the fact that at sufficiently high temperature, the hematite component in the manganese ore is reduced to magnetite which is strongly magnetic. This transformation is possibly done when the plasma heating is applied. After the plasma treatment, therefore, the grade of manganese ore can be improved using a magnetic separation.

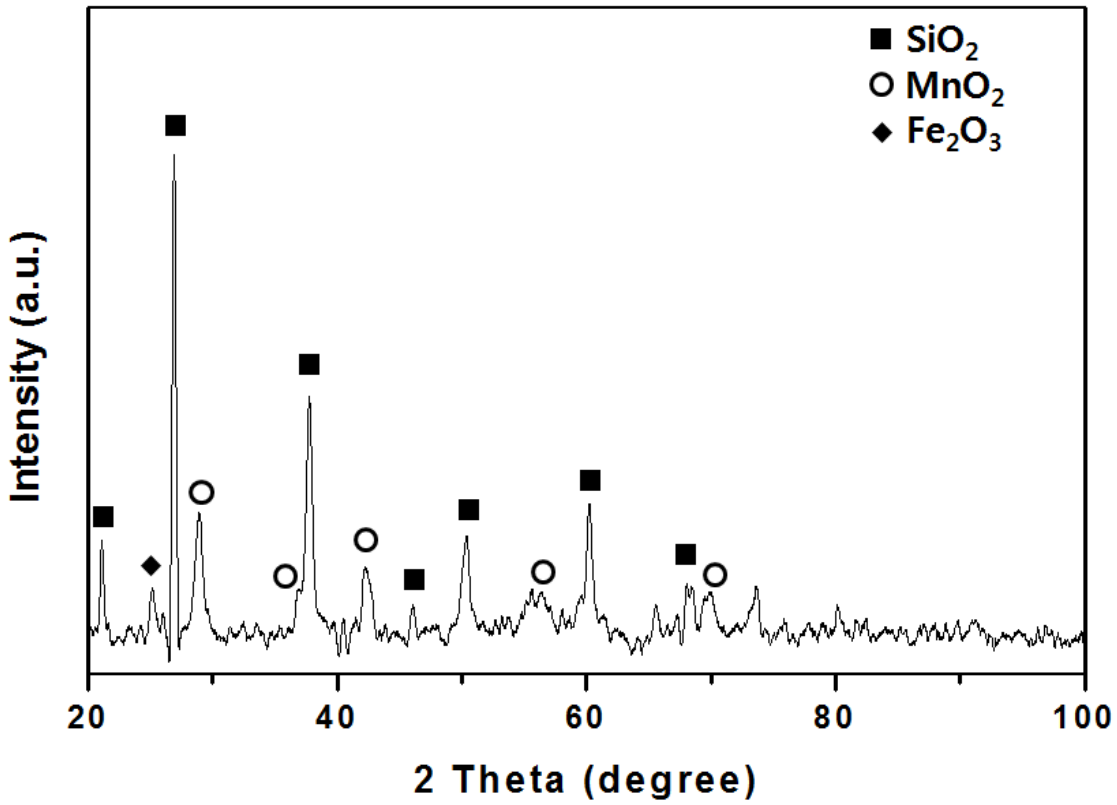


Figure 19. XRD patterns of the LP raw sample

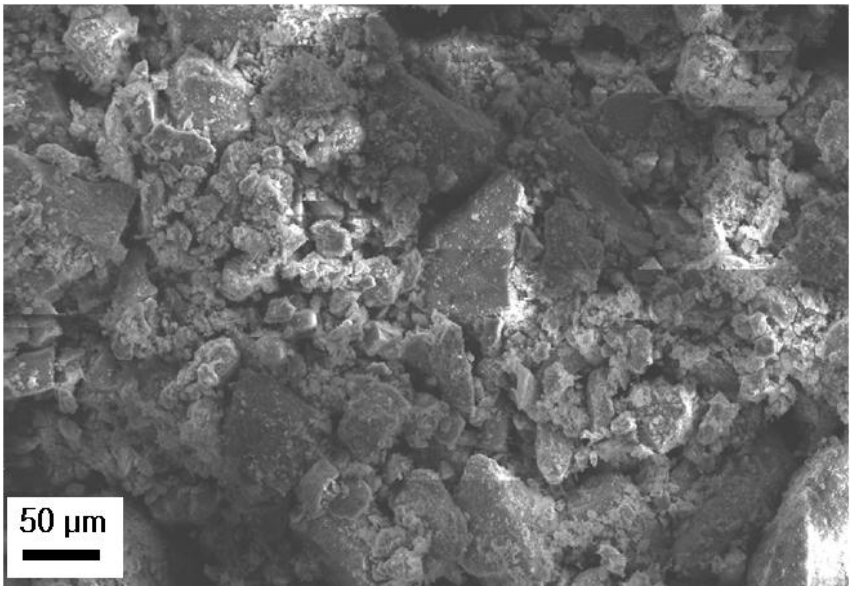


Figure 20. SEM micrograph of the LP raw sample

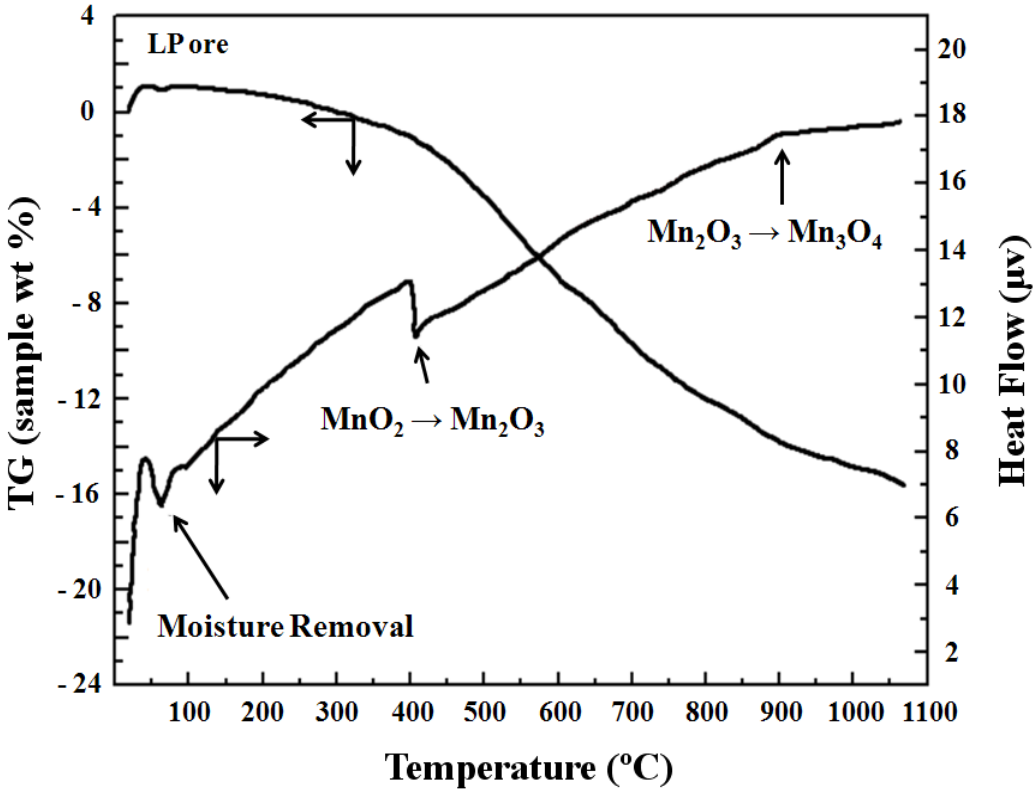


Figure 21. TG-DTA analysis of the LP raw sample (Heating rate 5°C/min)

When a weak magnet (0.032 Tesla, T) is used magnetic separation, the strong magnetic parts such as magnetite and metallic iron can be removed from both the weakly magnetic manganese oxide ($Mn_3O_4$) and the nonmagnetic manganese oxide ($MnO_2$, $Mn_2O_3$ and MnO). However, if too strong a magnet is used, the weak magnetic manganese oxide ($Mn_3O_4$) will be also removed (i.e. lost) together with magnetite and metallic iron.

In order to investigate the phase change after the plasma treatment, two experiments were carried out using Ar and Ar/$H_2$ mixture gases. The experimental conditions are listed in Table 14. Firstly, an experiment was carried with pure Ar gas (28.08 L/min, 25ºC, and 86.1 kPa) as the plasma gas to investigate the decomposition of the iron compound in the LP manganese ore. To improve the reduction rate of the oxide components, hydrogen gas was added (0.67 L/min, 25ºC, and 86.1 kPa) as a reductant in the second experiment. After the experiments, qualitative and quantitative analyses of phosphorus in the products were performed using SEM, EDS, and ICP. The phase transformation of the main components was analyzed by XRD patterns. The general aspects were the same as those observed in the case of H1 ore.

Table 14. Experimental conditions for the magnetic separation

| Torch power ( kW ) | Ar gas Flow Rate (L / min) | $H_2$ gas Flow Rate (L / min) | Powder Feed Rate (g/min) | Carrier gas Flow Rate (L/min) |
|---|---|---|---|---|
| 5.9 (Ar) | 28.1 | 0 | 2.1 | 2.1 |
| 6.3 (Ar+$H_2$) | 28.1 | 0.67 | 2.1 | 2.1 |

Figure 22 shows the XRD patterns after plasma treatment with Ar gas. It can be seen that the $MnO_2$ phases were transformed to $Mn_2O_3$ (JCPDS 24-0508), $Mn_3O_4$ (JCPDS 24-0734), and MnO (JCPDS 07-0230) due to thermal decomposition like in the case of H1 ore.

In addition, the thermal decomposition of $Fe_2O_3$ into $Fe_3O_4$ is also confirmed by the XRD analysis. $Fe_3O_4$ peaks overlapped, however, with $Mn_3O_4$ peaks, thus, it cannot be figured out easily after plasma treatment. Figure 23 shows the SEM micrograph of the plasma treated samples, both collected from the filter (Figure 23 a) and from the reactor (Figure 23 b). The SEM micrograph indicates that the shape was changed from an irregular shape to a spherical shape in the filtered product. As explained previously, fully melted dust changed to spherical shape during the plasma treatment.

Figure 24 shows the XRD patterns of the sample after plasma treatment with $Ar/H_2$ gases. The decomposition behavior of manganese oxides are almost the same as that observed with just Ar gas. In this case, however, it is confirmed that $Fe_2O_3$ in the ore was reduced to metallic Fe, because neither the XRD peak of $Fe_2O_3$ nor that of $Fe_2O_3$ was observed in both filtered and reactor products, and because the XRD peak of metallic Fe is observed in the XRD pattern of the reactor product. A possible reason why the XRD peak of metallic Fe was not observed in the filtered product is that $Fe_3O_4$ was reduced to FeO by $H_2$ and then combined with $SiO_2$ to form a melt (Figure 25 a) before further reduction to the metallic Fe. Once melted, the reduction is retarded. Figure 25 shows the SEM micrograph of the plasma treated samples both collected from the filter (Figure 25 a)) and the reactor (Figure 25 b)) after plasma treatment with $Ar/H_2$ gases. The irregular shape in the raw sample was changed to spherical shape in the filtered product.

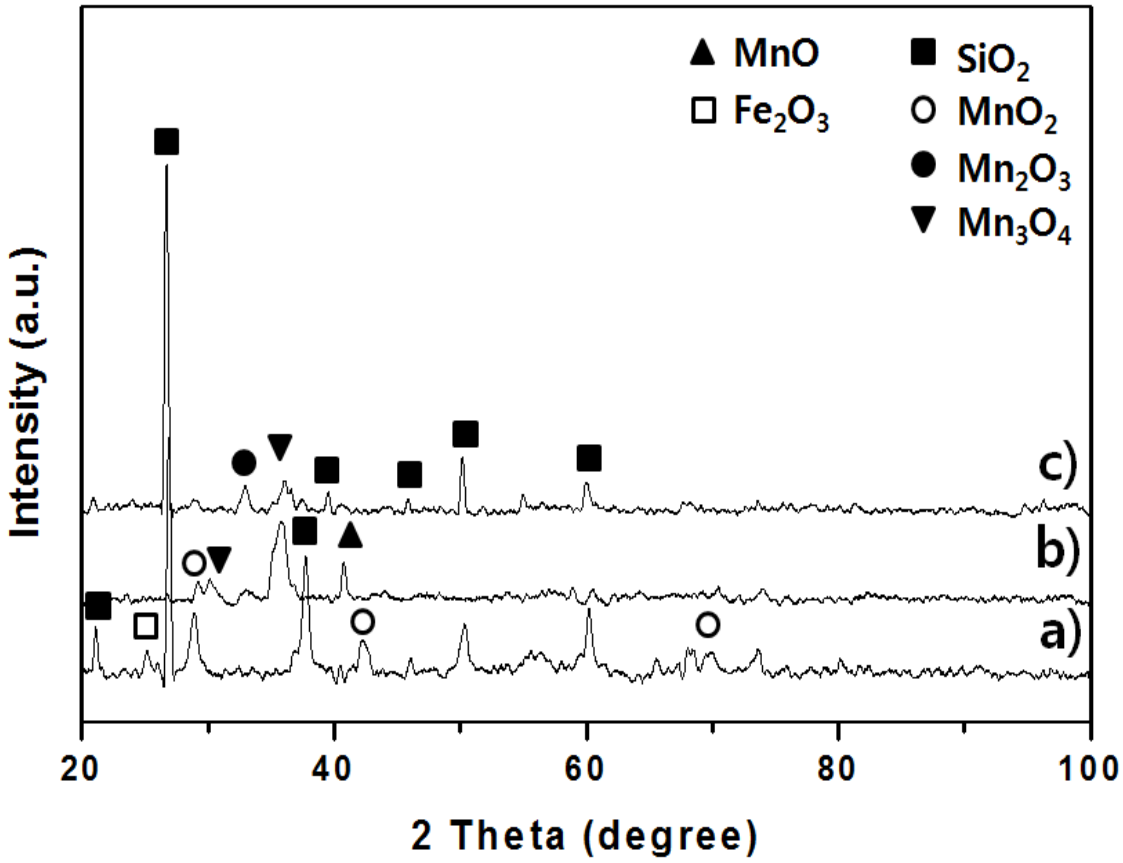


Figure 22. XRD patterns after plasma treatment with Ar gas for magnetic separation: a) LP raw sample, b) filtered product, and c) reactor product

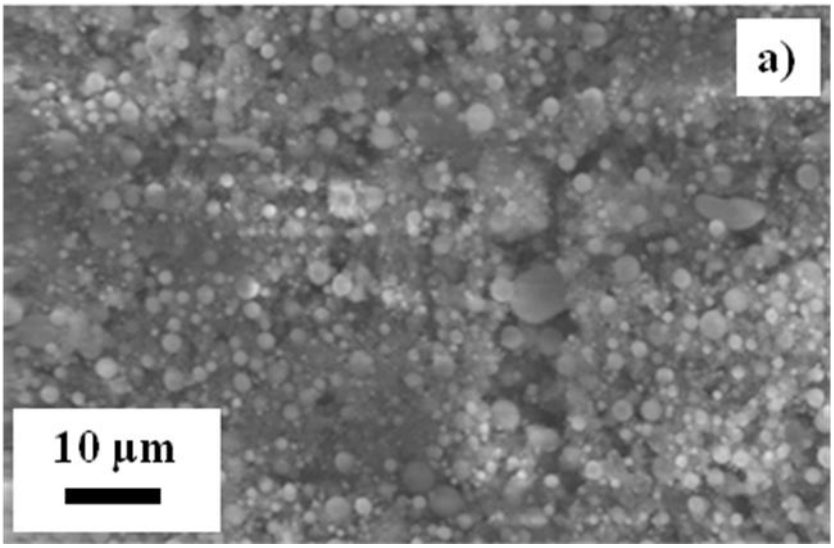


a)

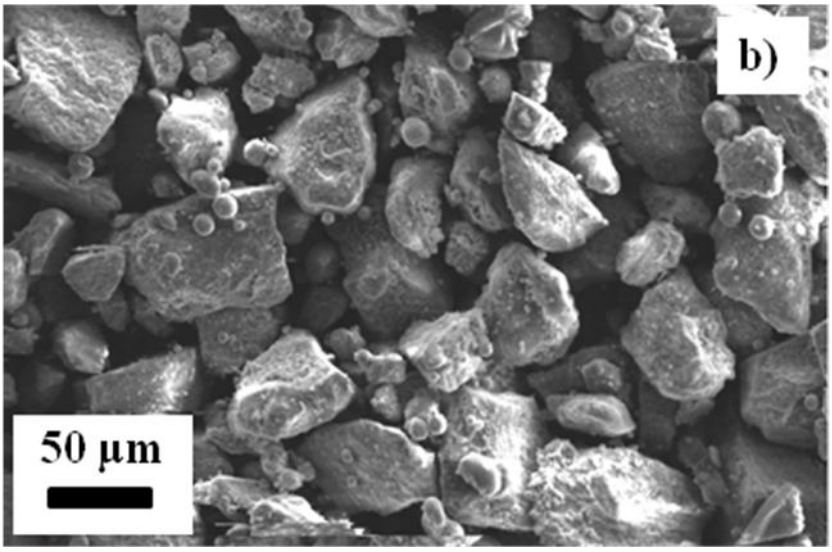


b)

Figure 23. SEM micrograph after plasma treatment with Ar gas for magnetic separation: a) filtered product, and b) reactor product

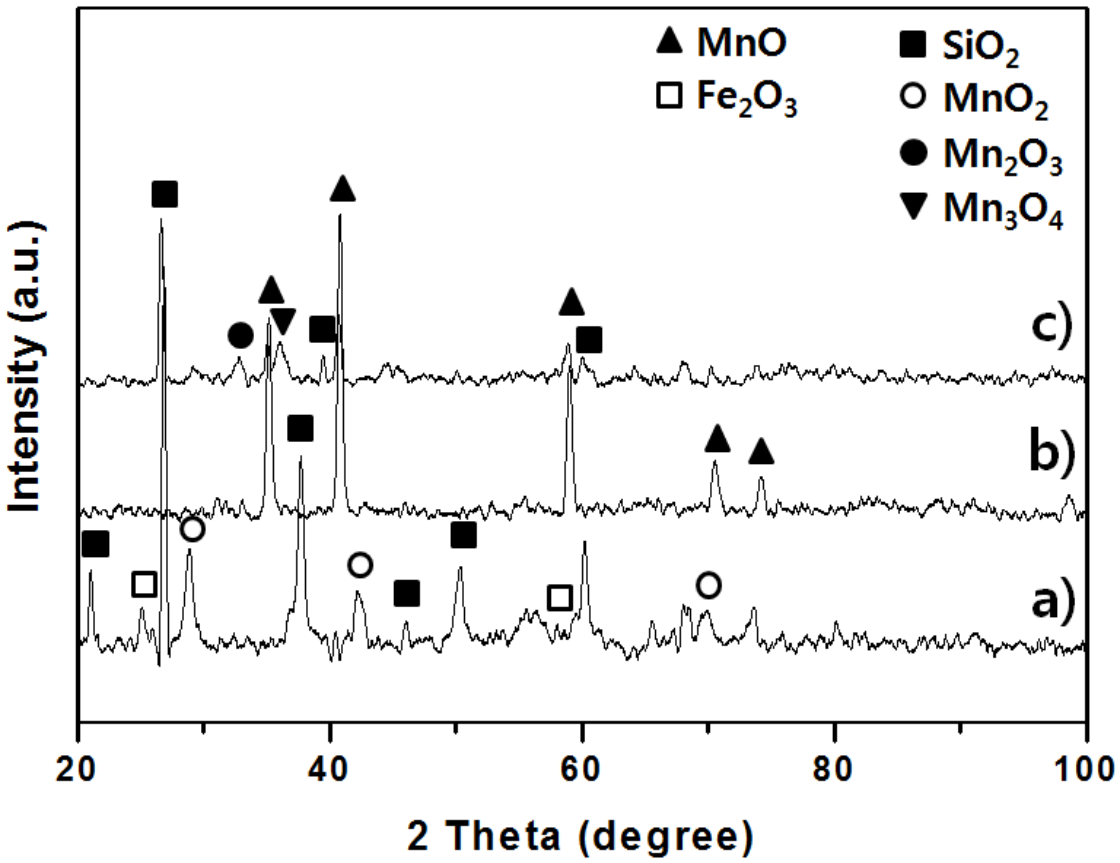


Figure 24. XRD patterns after plasma treatment with $Ar/H_2$ gases for magnetic separation: a) LP raw sample, b) filtered product, and c) reactor product

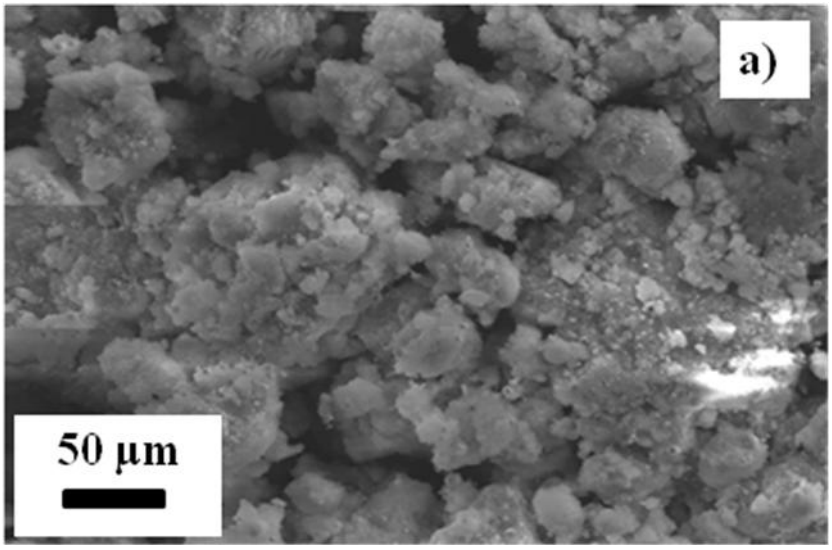


a)

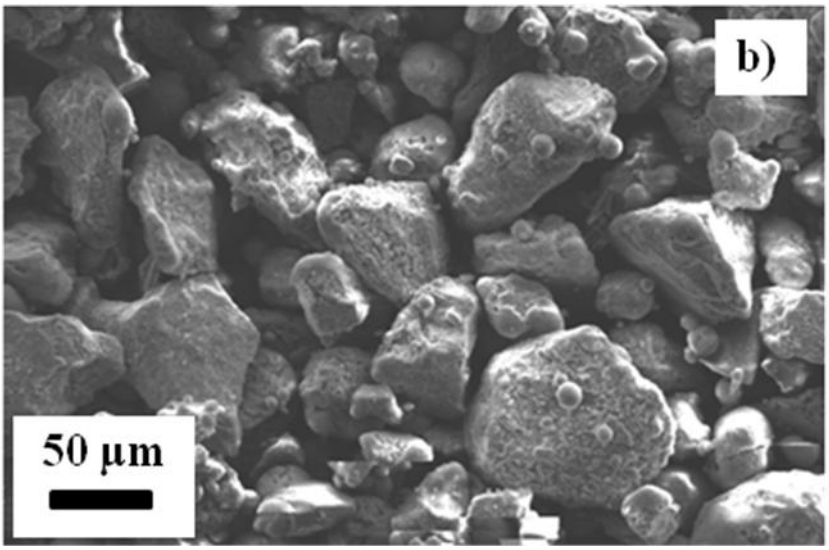


b)

Figure 25. SEM micrograph after plasma treatment with $Ar/H_2$ gases for magnetic separation: a) filtered product and b) reactor product

After the plasma treatment, the reactor product was subjected to two-stage magnetic separation by two magnets of 0.087 T and 0.032 T strengths. After the first magnetic separation by the stronger magnet (0.087 T), the magnetic part was put through second magnetic separation by the weaker magnet (0.032 T), as can be seen in Figure 26. In the first stage magnetic separation with the stronger magnet, magnetic components, both the weak magnetic components (such as $Mn_3O_4$, FeO, and $Fe_2O_3$) and the strong magnetic ones (such as $Fe_3O_4$ and metallic Fe), were separated from nonmagnetic components (such as $Mn_2O_3$, MnO, and $SiO_2$). After that, in the second stage magnetic separation with the weaker magnet, the strong magnetic components (such as $Fe_3O_4$ and metallic Fe) were separated from the weak magnetic components (such as $Mn_3O_4$, FeO, and $Fe_2O_3$). Finally, the weak magnetic components are combined with the nonmagnetic components to be the final product. Only the strong magnetic components such as $Fe_3O_4$ and metallic Fe are removed from the reactor product, and thereby, the grade of the reactor product is improved.

The results of magnetic separation after the plasma treatment according to the conditions in Table 14 were presented in Tables 15 and 16. As can be seen in the tables, the strong magnetic part considerably increased after the plasma treatment, especially when $H_2$ was added to the plasma gas. Theoretically, this increase can be obtained when $Fe_2O_3$ (weakly magnetic) was transformed to $Fe_3O_4$ or metallic Fe (strongly magnetic). In addition, nonmagnetic parts decreased after the plasma treatment. This decrease can be ascribe to the transformations of some of $MnO_2$ (nonmagnetic) to $Mn_3O_4$ (weakly magnetic). When $H_2$ is added to the plasma gas the nonmagnetic parts further decreased to around three-fourths. Because not all the above mentioned components are in separate

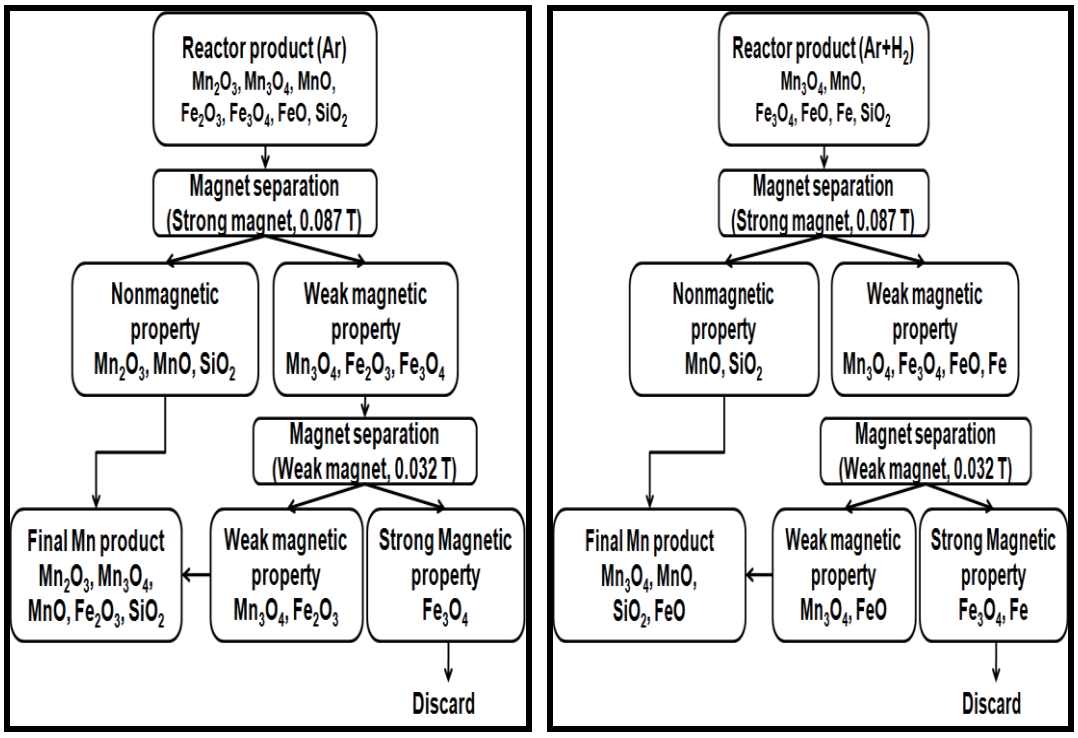


(a) (b)

Figure 26. Flow sheet for the removal of iron compound by strong and weak magnet: a) Ar reactor product and b) Ar/$H_2$ reactor product

free forms, the non-magnetic components that are attached to the magnetic ones or are in a compound form with the magnetic ones, can follow the magnetic portion. In addition, the separated components can be combined during the high temperature plasma treatment. Because of these complicated effects, further detailed or accurate quantitative analysis was difficult although the amount of the weak magnetic part increased.

Despite these problems, expected effects of the plasma treatment followed by magnetic separation on the upgrading of manganese ores were confirmed, as can be seen in Table 15. When only Ar gas is used as the plasma gas, the Fe wt% in the ore decreased from 2.3 % to 1.6 % and the Mn/Fe ratio increased from 18.6 to 30.3, and when hydrogen gas is added, the Fe wt% decreased to 1.6 % and the Mn/Fe ratio increased to 30.6.

Table 15. Mn, Fe wt%, and Mn/Fe ratio after magnetic separation

| | Nonmagnetic part | | | | Weak magnetic part (0.087 T) | | | | Strong magnetic part (0.032 T) | | | |
|---|---|---|---|---|---|---|---|---|---|---|---|---|
| | Mn (wt%) | Fe (wt%) | Mn/Fe | Weight (%) | Mn (wt%) | Fe (wt%) | Mn/Fe | Weight (wt%) | Mn (wt%) | Fe (wt%) | Mn/Fe | Weight (%) |
| Raw | 42.8 | 2.3 | 18.6 | 84.1 | 43.7 | 2.4 | 18.2 | 14.7 | 41.2 | 7.5 | 5.5 | 1.2 |
| Ar | 48.5 | 1.6 | 30.3 | 76.9 | 51.0 | 2.3 | 22.2 | 17.8 | 46.6 | 9.3 | 5.0 | 5.3 |
| Ar / $H_2$ | 48.9 | 1.6 | 30.6 | 61.4 | 52.5 | 1.9 | 27.6 | 28.6 | 49.7 | 7.0 | 7.1 | 9.9 |

Table 16. Mn, Fe wt%, and Mn/Fe ratio, recovery and loss % for final and removed product after magnetic separation

| | Final product | | | | | | Removed product | | | | | |
|---|---|---|---|---|---|---|---|---|---|---|---|---|
| | Mn (wt%) | Fe (wt%) | Mn/Fe | weight (%) | Recovery ( %) | | Mn (wt%) | Fe (wt%) | Mn/Fe | weight (%) | Loss ( %) | |
| | | | | | Mn | Fe | | | | | Mn | Fe |
| Raw | 42.4 | 2.3 | 18.4 | 98.8 | 97.6 | 95.6 | 41.2 | 7.5 | 5.5 | 1.2 | 2.4 | 4.4 |
| Ar | 46.4 | 1.6 | 29.0 | 94.7 | 90.0 | 71.0 | 46.6 | 9.3 | 5.0 | 5.3 | 10.0 | 29.0 |
| $Ar+H_2$ | 45.0 | 1.5 | 30.0 | 90.1 | 81.1 | 60.9 | 49.7 | 7.0 | 7.1 | 9.9 | 18.9 | 39.1 |

The recovery and loss percentages for the final and removed products are given in Table 16. When Ar gas is used as the plasma gas, the recovery % of Mn decreased from 97.6 to 90.0 % and the loss % of Fe increased from 4.4 to 29.0 %. When hydrogen gas is added, the recovery of Mn decreased to 81.1 % and the loss of Fe increased to 39.1 %.

Figure 27 shows the effect of magnetic force on the magnetic separation after the plasma treatment. When the strong magnet (0.087 T) is used, the separation was found to be poor because the weak magnetic component $Mn_3O_4$ was also attracted to the magnet together with the strong magnetic components $Fe_3O_4$ and Fe, which caused an excess loss of manganese to tailing. When the weak magnet (0.032 T) is used, however, the separation was successfully done without a significant loss of manganese to tailing, because in this case, only the strong magnetic components $Fe_3O_4$ and Fe were selectively attracted to the magnet.

As the overall results, when only Ar gas is used as the plasma gas, the Fe contents were increased to 29%, and when hydrogen gas is added, the Fe contents were increased to 39.1. Also, for making standard high carbon ferromanganese, the Mn:Fe ratio should be a minimum of 6 as explained in the literature review section. Based on the results, Table 15 and 16, the Mn/Fe ratio increased to 30 when hydrogen gas added. Therefore, magnetic separation after plasma treatment for upgrading of manganese ore is effective. In other words, manganese ore was upgraded by removal of Fe contents after plasma treatment.

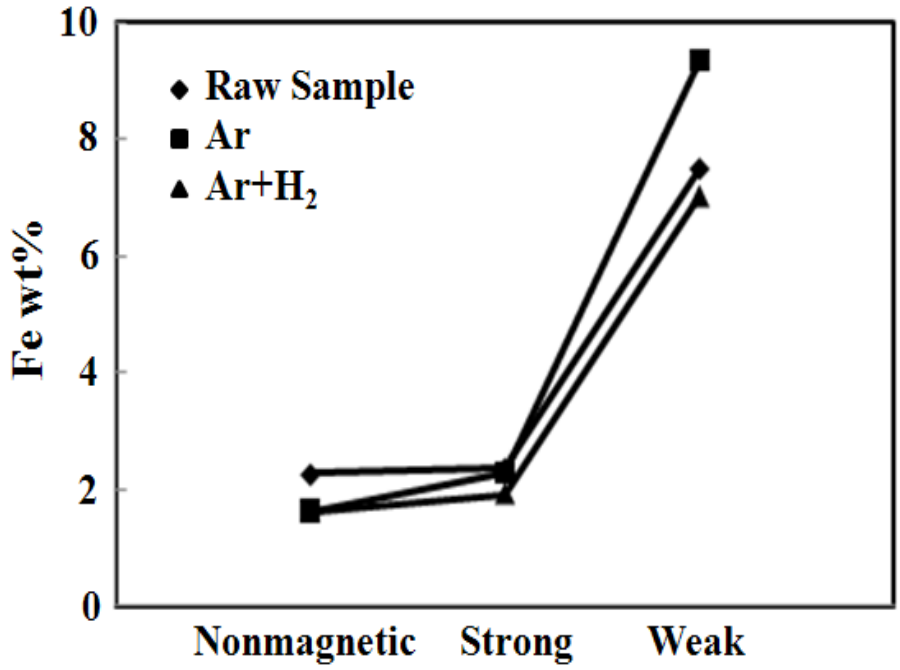


a)

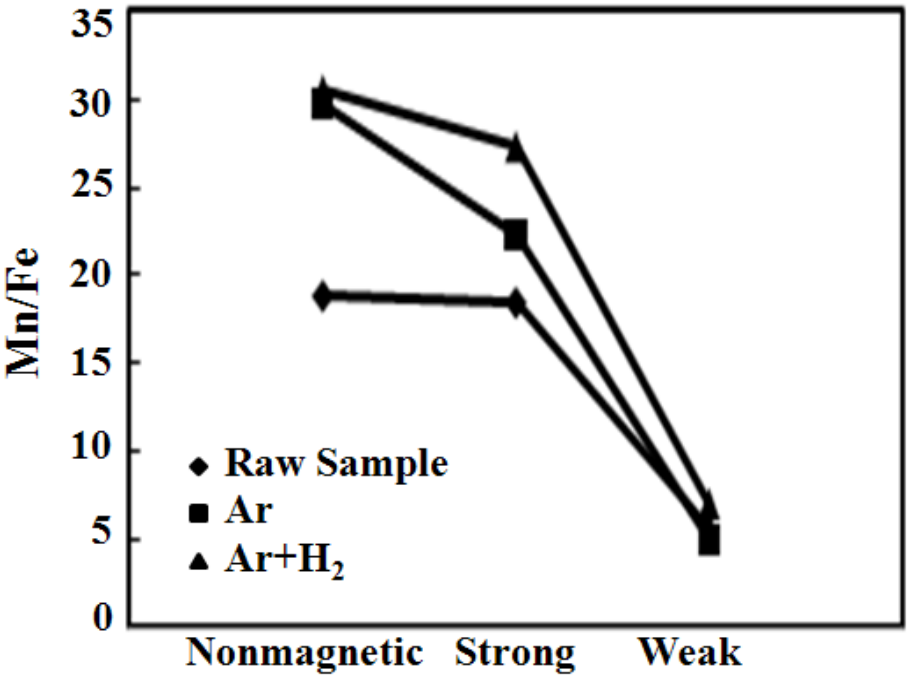


b)

Figure 27. Magnetic separation results: (a) Fe wt% and (b) Mn/Fe ratio

## 5. SUMMARY AND CONCLUSIONS

As an alternative technology for the dephosphorization in the manganese smelting process, the vaporizing removal of phosphorus compounds directly from manganese ores at very high temperatures was investigated in this study using a plasma system. For the removal of phosphorus, the effects of argon gas flow rate, $H_2$ content in the plasma gas, and plasma torch power were determined. In addition, based on the thermal decomposition or reduction of hematite in the ore to magnetite at a high temperature, magnetic separation was conducted after plasma treatment to upgrade manganese.

For the removal of the phosphorus, low Ar gas flow rate and high torch power were found to be effective, and the use of hydrogen gas as a reducing agent was beneficial to the ores. For the upgrading of manganese ore, when the strong magnet (0.087 T) is used, magnetic separation after the plasma treatment was found to be poor because the weakly magnetic component $Mn_3O_4$ was also attracted to the magnet together with the strong magnetic components $Fe_3O_4$ and Fe. However, when a weak magnet (0.032 T) is used, better separation was achieved without a significant loss of manganese to tailing, because in this case, only the strong magnetic components $Fe_3O_4$ and Fe were selectively attracted to the magnet.

# APPENDIX

## SUMMARY OF EXPERIMENTAL DATA

A. Direct removal of the phosphorus by plasma treatment

a) Feasibility of the plasma treatment

| Torch power (kW) | Plasma gas flow rate (L/min, at 25 ºC and 86.1 kPa) | | Feeding rate (g/min) | Carrier gas (L/min) | Results |
|---|---|---|---|---|---|
| | Ar | $H_2$ | | | |
| 5.9 | 28.1 | 0 | 2.25 | 2.1 | The application of plasma for the removal of phosphorus directly from the raw manganese ores is feasible, especially when hydrogen is added to the plasma gas as a reductant. |
| 6.78 | 28.1 | 0.67 | 2.22 | 2.1 | |

b) Effect of the Ar gas flow rate

| Torch power (kW) | Plasma gas flow rate (L/min, at 25 ºC and 86.1 kPa) | | Feeding rate (g/min) | Carrier gas (L/min) | Results |
|---|---|---|---|---|---|
| | Ar | $H_2$ | | | |
| 5.9 | 21.4 | - | 2.14 | 2.1 | When the argon gas flow rate increased, the P/Mn ratio in the filtered product decreased while that in the reactor product rather increased. This can be ascribed to the shorter residence time and the lower plasma flame temperature with the increase of the flow rate of argon gas. |
| 5.9 | 28.1 | - | 2.22 | 2.1 | |
| 5.9 | 34.8 | - | 2.14 | 2.1 | |

c) Effect of the $H_2$ gas flow rate

| Torch power (kW) | Plasma gas flow rate (L/min, at 25 ºC and 86.1 kPa) | | Feeding rate (g/min) | Carrier gas (L/min) | Results |
|---|---|---|---|---|---|
| | Ar | $H_2$ | | | |
| 5.9 | 28.1 | 0 | 2.25 | 2.1 | The addition of hydrogen to the plasma gas clearly showed a positive effect on the dephosphorization, but there was an optimum point. One thing that should be noticed is that the use of hydrogen can cause the formation of toxic phosphene ($PH_3$), although the generated amount of phosphene during the plasma treatment is expected to be negligibly small. |
| 6.3 | 28.1 | 0.06 | 2.1 | 2.1 | |
| 6.78 | 28.1 | 0.67 | 2.22 | 2.1 | |

d) Effect of the plasma torch power

| Torch power (kW) | Plasma gas flow rate (L/min, at 25 ºC and 86.1 kPa) | | Feeding rate (g/min) | Carrier gas (L/min) | Results |
|---|---|---|---|---|---|
| | Ar | $H_2$ | | | |
| 5.9 | 28.1 | - | 1.19 | 3.15 | The dephosphorization, clearly increased with an increase of the torch power without any significant loss of manganese into off gas (and dust). As a conclusion, for the improvement of the dephosphorization by plasma treatment, an increase of torch power is more desirable than an increase of $H_2$ content in the plasma gas because of $PH_3$ generation. |
| 8.5 | 28.1 | - | 1.14 | 3.15 | |
| 11.8 | 28.1 | - | 1.17 | 3.15 | |
| 14.9 | 28.1 | - | 1.14 | 3.15 | |

B. Upgrading of a manganese ore by plasma treatment

a) Magnetic separation

| Torch power (kW) | Plasma gas flow rate (L/min, at 25 ºC and 86.1 kPa | | Feeding rate (g/min) | Carrier gas (L/min) | Results |
|---|---|---|---|---|---|
| | Ar | $H_2$ | | | |
| 5.9 | 28.1 | 0 | 2.1 | 2.1 | The strong magnetic part considerably increased after the plasma treatment, especially when $H_2$ was added to the plasma gas. Expected effects of the plasma treatment followed by magnetic separation on the upgrade of the manganese ores were obviously confirmed. |
| 6.3 | 28.1 | 0.67 | 2.1 | 2.1 | |

## REFERENCES


1. W. Zhang and C. Yong. Cheng, "Manganese Metallurgy Review. Part I: Leaching of ores/ Secondary Materials and Recovery of Electrolytic/ Chemical Manganese Dioxide," *Hydrometallurgy*, **89**, 137-59 (2007).

2. T. Kaneko, T. Matsuzaki, T. Kugimiya, K. Ide, M. Kumakura, and A. Kasama, "Improvement of Mn Yield in Less Slag Blowing at BOF by Use of Sintered Manganese Ore," *Journal of the Iron and Steel Institute of Japan*, **79** [8] 941-7 (1993).

3. R. L. Parker, "Composition of the Earth's Crust," In *Data of Geochemistry*, 6th Edition, Professional Paper 440-D, Edited by M. Fleischer, USGS, Reston, VA, 1967.

4. J. Gutzmer and N. J. Beukes, "Mineral Paragenesis of the Kalahari Manganese Field, South Africa," *Ore Geology Reviews*, **11** [6] 405-28 (1996).

5. T. Arato, T. Uchida, and Y. Omori, "Reducing Dephosphorization of Molten Stainless Steel by Metallic Calcium," *Transactions ISIJ*., **25**, 326-32 (1985).

6. Z. H. Tian, B. H. Li, X. M. Zhang, and Z. H. Jiang, "Double Slag Operation Dephosphorization in BOF for Producing Low Phosphorus Steel," *Journal of Iron and Steel Research, International*, **16** [3] 6-14 (2009).

7. H. Tanabe and M. Nakada, "Steelmaking Technologies Contributing to Steel Industries," NKK Technical Review, **88**, 18-27 (2003).

8. C. Akil and A. Geveci, "Optimization of Conditions to Produce Manganese and Iron Carbides from Denizli-Tavas Manganese Ore by Solid State Reduction," *Turkish J. Eng. Env. Sci*., **32**, 125-31 (2008).

9. G. G. Roy, P. N. Chaudhary, R. K. Minj, and R. P. Goel, "Dephosphorization of Ferromanganese using $BaCO_3$ based Fluxes by Submerged Injection of Powders: A Preliminary Kinetic Study," *Metallurgical and Materials Transactions B*., **32B**, 558-61 (2001).

10. M. I. Boulos, "Radio Frequency Plasma Developments; Scale Up and Industrial Application," *J. High Temperature Chemical Processes*, **1**, 401-11 (1992).

11. J. Jurewicz and M. I. Boulos, "High Energy Density Induction Plasma System for Materials Processing," 5th National Thermal Spray Conference (NTSC): Thermal Spray Industrial Application, Anaheim, CA, 89-95 (1993).

12. M. I. Boulos and J. Jurewicz, "High Performance Induction Plasma Torch with a Water-Cooled Ceramic Confinement Tube"; U.S. Patent 5 200 595, April 6, 1993.

13. R. H. Smith and R. Novak, "Advances and Applications in U.S. Thermal Spray Technology I: Technology and materials," *Powder Metallurgy International*, **23**, 147-55 (1991).

14. M. I. Boulos, "R.F. Induction Plasma Spraying, State of the Art Review," *J. of Thermal Spray Technology*, **1**, 33-40 (1992).

15. K. Mizuno, W. Takeshige, K. Yutaka, A. Reiji, K. Satoshi, K. Satoru, O. Hideo, Y. Toyonobu, K. Yoshiro, A. Takanobu, K. Hisashi, and H. Shoji, "Apparatus for Decomposing Halogenated Organic Compound"; U.S. Patent 5 187 344, February 16, 1993.

16. L. Tong and R. G. Reddy, "Synthesis of Titanium Carbide Nano-powders by Thermal Plasma," *Scr. Mater.*, **52**, 1253-8 (2005).

17. D. Elanski, J. W. Lim, K. Mimura, and M. Isshiki, "Impurity Removal from Zr, Nb and Ta Metals by Hydrogen Plasma Arc Melting and Thermodynamic Estimation of Hydride Formation," *Journal of Alloys and Compounds*, **413**, 251–8 (2006).

18. A. E. Elsherief, "A Study of the Electroleaching of Manganese Ore," *Hydrometallurgy*, **55** [3] 311-26 (2000).

19. U. S. Geological Survey, Mineral Commodity Summaries, January 2011.

20. T. S. Jones, "Manganese," from Minerals Yearbook, Metals and Minerals, U.S. Bureau of Mines, **1**, 789-812 (1992).

21. American Society for Testing and Materials (ASTM), Iron and Steel Products in *Annual Book of ASTM Standards*, Volume 01, 02, Standard Speciations A99-82 (ferromanganese); A483-64 (silico-manganese); and A701-96 (ferromanganese-silicon). ASTM International, PA; West Conshohocken, 1998.

22. C. Y. Cheng, V. N. Misra, J. Clough, and R. Muni, "Dephosphorization of Western Australian Iron Ore by Hydrometallurgical Process," *Minerals Engineering*, **12** [9] 1083-92 (1999).

23. A. L. Groshkova, L. A. Polulyakh, A. Y. Travyanov, V. Y. Dashevskii, and Y. S. Yusfin, "Phosphorus Distribution between Phases in Smelting High-Carbon Ferromanganese in the Blast Furnace," ISSN 0967-0912, *Steel in Translation*, **37** [11] 904–7 (2007).

24. R. P. Goel and S. Srikanth, "A Thermodynamic Analysis of Ferromanganese," paper presented at the 46th Annual Technical Meeting of Indian Institute of Metals, held in Udaipur, India, November 14-17, 1992.

25. J. F. Elliott, M. Gleiser, and V. Ramakrishna, *Thermochemistry for Steelmaking*. Addison-Wesley, NY, 1961.

26. X. liu, O. Wijk, R. Salin, and J. O. Edstrom, "Phosphorus Equilibrium between BaO-$BaF_2$-MnO Fluxes and Ferromanganese Melts," *Steel Research*, **66** [3] 90-102 (1995).

27. P. N. Chaudhary and R. P. Goel "Dephosphorization of Liquid Ferromanganese," paper presented during 4th refresher course on Ferro Alloy, held in Jamshedpur, India, January 12-14, 1994.

28. P. N. Chaudhary, R. P. Goel, R. K. Minj, and S. B. Sarkar, "A Flux Based Dephosphorization Process for High Carbon Liquid Ferromanganese," paper presented during national seminar on Ferro Alloys present and future held in Jamshedpur on 5-6th May, 1995 organized by Tata Steel and Indian Institute of Metals chapter Jamshedpur, India.

29. P. N. Chaudhary, R. P. Goel, and R. K. Minj, CSIR Patent application No 2459 / DEL / 95 dated 29 / 12 / 95.

30. P. N. Chaudhary, "Dephosphorization of High Carbon Ferromanganese Using $BaCO_3$ Based Fluxes," PhD thesis, Indian Institute of Technology, Kharagpur, India, March 2000.

31. P. N. Chaudhary, R. P. Goel, and G. G. Ray, "Dephosphorization of High Carbon Ferromanganese Using Barium Carbonate-based Fluxes, a Feasibility Study," *Ironmaking and Steelmaking*, **28** [5] 396-403 (2001).

32. A. I. Zaitsev, N. V. Korolyov, and B. M. Mogutnov, "Thermodynamic Properties of xCa + (1 − x)P," *The Journal of Chemical Thermodynamics*, **23** [1] 11-23 (1991).

33. Y. Watanabe, K. Kitamura, F. Rache, T. Sukihaski, and N. Sano, "Thermodynamics of Phosphorus and Sulfur in the BaO-MnO Flux System between 1573 and 1673 K," *Met. Trans B.*, **20B**, 339-47 (1993).

34. Y. Nakamura, K. Harashima, and M. Itoh, "Phosphorus Removal from Fe-Cr-C Alloys with $CaC_2$-$CaF_2$ Flux," *Journal of the Iron and Steel Institute of Japan*, **63**, 2287-91 (1977).

35. N. Masumitsu, K. Ito, and R. J. Fruehan, "Thermodynamics of Ca-$CaF_2$ and Ca-$CaCl_2$ Systems for Dephosphorization of Steel," *Met. Trans B.,* **19** [4] 643-8 (1988).

36. Y. Nakamura, N. Tokumitsu, K. Harashima, and K. Segawa, "Refining of 18% Chromium-8% Nickel Steel with Calcium-Calcium Fluoride Solution," *Transactions of the Iron and Steel Institute of Japan*, **16**, 623-7 (1976).

37. H. Katayama, H. Kajioka, K. Harashima, and M. Inatomi, "Dephosphorization of High Chromium Molten Steel with $CaC_2$-$CaF_2$ Flux," *Transactions of the Iron and Steel Institute of Japan,* **19** [10] 635-43 (1979).

38. L. F. Pfender, "Trends in Thermal Plasma Technology," *Thermal Plasma Torches and Technologies*, **1**, 20-41(2000).

39. R. M. Young and L. F. Pfender, "Generation and Behavior of Fine Particles in Thermal Plasmas-A Review," *Plasma Chemistry and Plasma Processing*, **5**, 1-37 (1985).

40. S. K. Friedlander, "Synthesis of Nanoparticles and their Agglomerates: Aerosol Reactors," R&D Status and Trends in Nanoparticles, Nanostructured Materials, and Nanodevices in the United States, Proceedings of the, May 8-9, MD, 1997.

41. V. Subramanian, R. Baskaran, and H. Krishnan, "Thermal Plasma Synthesis of Iron Oxide Aerosols and Their Characteristics," *Aerosol and Air Quality Research*, **9** [2] 172-86 (2009).

42. J. Heberlein, "New Approaches in Thermal Plasma Technology," *Pure Appl. Chem*., **74** [3] 327-35 (2002).

43. K. P. Sreekumar, P. V. Ananthapadmanabhan, N. Venkaramani, A. Khan, P. V. Joshi, V. D. Sawant, and Y. S. Mayya, "Aerosol Generation by Thermal Plasma Technique," *Indian Aerosol Science and Technology Association Bulletin*, **3**, 110 (2000).

44. N. Venkataramani, "Industrial Plasma Torches and Application," *Curr. Science*, **83**, 254-62 (2002).

45. F. E. Kruis, H. Fissan, and A. Peled, "Synthesis of Nanoparticles in the Gas Phase for Electronic," Optical and Magnetic Applications: A Review. *J. Aerosol Sci*., **29**, 511-35 (1998).

46. P. Fauchais and A. Vardelle, "Pending Problems in Thermal Plasmas and Actual Development," *Plasma Physics Controlled Fusion*, **42**, 365–83 (2000).

47. K. Mimura, S. W. Lee, and M. Isshiki, "Removal of Alloying Elements from Zirconium Alloys by Hydrogen Plasma-arc Melting," *J. of Alloys and Compounds*., **221**, 267-73 (1995).

48. O. Auciello and D. L. Flamm, *Plasma Diagnostics, Plasma Materials Interactions*. Academic Press, CA, 1989.

49. M. I. Boulos, "New Frontiers in Thermal Pasma Processing," *Pure Appl. Chem*., **68**, 1007–10 (1996).

50. G. Bonizzoni, and E. Vassallo, "Plasma Physics and Technology; Industrial Applications," *Vacuum*, **64**, 327–36 (2002).

51. P. C. Kong and Y. C. Lau, "Plasma Synthesis of Ceramic Powders," *Pure & App. Chem*., **62** [9] 1809-16 (1990).

52. E. Gormez, D. A. Rani, C. R. Cheeseman, D. Deegan, M. Wise, and A. R. Boccaccini, "Thermal Plasma Technology for the Treatment of Wastes: A Critical Review," *J. Hazard. Mater*., **161** [2] 614-26 (2009).

53. L. A. Polulyakh, V. Ya. Dashevskii, A. Ya. Travyanov, Yu. S. Yusfin, and A. L. Petelin, "Behavior of Phosphorus in the Blast Furnace in Smelting Hot Metal and Ferromanganese," ISSN 0967-0912, *Steel in Translation*, **39** [3] 187–9 (2009).

54. K. S. Hwang, "Chemical Vapor Synthesis of Tungsten Nanopowder in Thermal Plasma and Its Sintering Behavior," M. S. Thesis, University of Utah, Salt Lake City, Utah, 2008.